

Computing the complex

Dusty plasmas in the presence of magnetic fields and UV radiation

Berekenen van het complex(e)
Stoffige plasma's in de aanwezigheid van magnetische velden en
ultraviolette straling

(met een samenvatting in het Nederlands)

PROEFSCHRIFT

ter verkrijging van de graad van doctor aan de Universiteit Utrecht, op
gezag van de rector magnificus, prof. dr. J.C. Stoof, ingevolge het
besluit van het college voor promoties in het openbaar te verdedigen op
dinsdag 11 december 2007 des ochtends te 10.30 uur

door

Victor Land

geboren op 25 december 1979, te Zijpe

Promotoren: Prof. Dr. W. J. Goedheer
Prof. Dr. N. J. Lopes Cardozo

The work described in this thesis was performed as part of the research programme of the ‘Stichting voor Fundamenteel Onderzoek der Materie’ (FOM) with financial support of the ‘Nederlandse Organisatie voor Wetenschappelijk Onderzoek’ (NWO), and Euratom, and with financial support from the CPS research school.

List of natural constants, used symbols and acronyms

Symbol	Name	Value	[]
Natural constants			
ϵ_0	Permittivity of vacuum	$8.85419 \cdot 10^{-12}$	F m ⁻¹
κ_T	Thermal conductivity coefficient	$1.772 \cdot 10^{-2}$ (Ar)	W K ⁻¹ m ⁻¹
c	Speed of light in vacuum	299 792 458	m s ⁻¹
e	Natural number	2.71828	–
e	Electron charge	$1.60219 \cdot 10^{-19}$	C
h	Planck constant	$6.62618 \cdot 10^{-34}$	J s
k_B	Boltzmann constant	$1.38066 \cdot 10^{-23}$	J K ⁻¹
m_e	Electron mass	$9.10953 \cdot 10^{-31}$	kg
m_p	Proton mass	$1.67265 \cdot 10^{-27}$	kg
m_+	Argon-18 ion mass	$6.633645 \cdot 10^{-26}$	kg
Fields and potentials			
B	Magnetic induction	–	T
E	Electric field	$-\nabla\phi(r)$	V m ⁻¹
$\bar{\mathbf{E}}$	Time averaged electric field	–	V m ⁻¹
\mathbf{E}_{eff}	Effective electric field	–	V m ⁻¹
$E_{k+\frac{1}{2}}$	Electric field at midpoint (PIC)	$\frac{V_k - V_{k+1}}{\Delta z}$	V m ⁻¹
F	General force	–	N
F_E	Electrostatic force	–	N
F_g	Force of gravity	–	N
F_{ion}	Ion drag force	–	N
F_{nd}	Neutral drag force	–	N
F_{th}	Thermophoretic force	–	N
g	Gravitational acceleration	$-9.81 \hat{z}$	m s ⁻²
L	Angular momentum	$m\mathbf{r} \times \mathbf{v}$	kg m ² s ⁻¹
$\phi(r)$	Potential	–	V
ϕ_D	Dust particle surface potential	$Q_D/4\pi\epsilon_0 R$	V
Ψ	Effective potential	$e\phi(r)/T_e(eV)$	–
Ψ_D	Effective dust particle potential	$e\phi_D/T_e(eV)$	–
V_a	Anode potential	–	V
V_c	Cathode potential	–	V
V_f	Measured floating potential	–	V
V_k	Potential on grid point k (PIC)	–	V
V_p	Measured plasma potential	–	V

Symbol	Name	Value	[]
--------	------	-------	-----

Length scales and cross sections

Δ	Average inter-particle distance	$n^{-1/3}$	m
λ_D	Linearized Debye length	$(1/\lambda_e^2 + 1/\lambda_+^2)^{-1/2}$	m
λ_e	Electron Debye length	$(\epsilon_0 k_B T_e / e^2 n_e)^{1/2}$	m
λ_+	Ion Debye length	$(\epsilon_0 k_B T_+ / e^2 n_+)^{1/2}$	m
ρ_0	Coulomb radius	$R(e\phi_D / 2E_s)$	m
σ	General collision cross section	–	m ²
σ_{abs}	Light absorption cross section	–	m ²
σ_c	OML collection cross section	πb_c^2	m ²
σ_{ext}	Light extinction cross section	–	m ²
σ_s	Ion momentum scattering cross section	$4\pi\rho_0^2\Lambda$	m ²
σ_{sca}	Light scattering cross section	–	m ²
A_S	Sheath surface area	–	m ²
L_{NN}	Distance between nearest neighbors	–	m
R	Dust particle radius	–	m
b_c	OML collection radius	$R(1 - e\phi_D / E_s)^{1/2}$	m
h	Impact parameter	–	m
l_{mfp}	Mean free path	$(n\sigma)^{-1}$	m
r_c	Cyclotron radius	v_\perp / ω_c	m

Time scales, rates, frequencies, currents

Γ_j	Flux of particle species j	–	m ⁻² s ⁻¹
Γ_{w_e}	Flux of electron energy density	–	J m ⁻² s ⁻¹
ν	General collision frequency	–	s ⁻¹
ν_{RF}	RF frequency	$13.56 \cdot 10^6$	s ⁻¹
ν_+	Ion momentum transfer frequency	$e / m_+ \mu_+$	s ⁻¹
$\langle \sigma v \rangle$	Ionization rate	–	m ³ s ⁻¹
τ_{ch}	Charging time	$\frac{\epsilon_0 (2m_+ E_s)^{1/2}}{e^2 R n_+}$	s
τ_{it}	Ion transit time	$(eV_c / k_B T_e)^{3/4} \omega_{p,+}^{-1}$	s
$\tau_{p,D}$	Dust acoustic wave period	$2\pi / \omega_{p,D}$	s
τ_{RF}	RF period	$1 / \nu_{RF}$	s
$\omega_{c,j}$	Cyclotron frequency for species j	$q_j \mathbf{B} / m_j$	rad s ⁻¹
$\omega_{p,j}$	Plasma frequency for species j	$(n_j Z_j e^2 / m_j \epsilon_0)^{1/2}$	rad s ⁻¹
\mathcal{F}	Flux	–	m ⁻² s ⁻¹
\mathcal{I}	Intensity of light source	–	W m ⁻²
I_j, J_j	Current (density) of species j	–	C s ⁻¹ (m ⁻²)
I_{is}, J_{is}	Ion saturation current (density)	–	C s ⁻¹ (m ⁻²)
S_j, S_{w_e}	Sinks or source term for particles/energy	–	(J) m ³ s ⁻¹
k_{rec}	Volume recombination rate	–	m ³ s ⁻¹

Symbol	Name	Value	[]
Dusty plasma parameters			
Γ	Coupling parameter	$\frac{Q_D^2 \exp(-\Delta/\lambda_D)}{4\pi\epsilon_0\Delta k_B T_D}$	–
Λ	Coulomb logarithm	$\ln\left(\frac{1+\beta}{\beta+R/\lambda_D}\right)$	–
α	Mass ratio	m_+/m_e	–
β	Non-linearity parameter	ρ_0/λ_D	–
μ_j	Mobility for charged species j	$Z_j e/m_j \nu_{m,j}$	$\text{m}^2 (\text{Vs})^{-1}$
ρ	Charge density	$\Sigma_j (n_j Z_j e)$	C m^{-3}
σ_p	Particle surface charge density	$Q_D/4\pi R^2$	C m^{-2}
\mathcal{K}	Collisional operator in ion drag	–	–
\mathcal{P}	Havnes parameter	$n_D Z_D/n_e$	–
D_a	Ambipolar diffusion coefficient	$\frac{\mu_+ D_e + \mu_e D_+}{\mu_e + \mu_+}$	$\text{m}^2 \text{s}^{-1}$
D_j	Diffusion coefficient for species j	$\mu_j k_B T_j / Z_j e$	$\text{m}^2 \text{s}^{-1}$
H_j	Hall parameter for species j	$\omega_{c,j} / 2\pi \nu_{m,j}$	–
N_j	Particle number of species j	$n_j \times \text{Volume}$	–
N_{NN}	Number of nearest neighbors	–	–
P_j	Partial pressure of species j	$n_j k_B T_j$	Pa
Q_D	Dust charge	$Z_D e$	C
T_j	Temperature of species j	–	K
Z_j	Charge number for species j	–	–
n_j	Number density of species j	–	m^{-3}
x_j	Fractional ionization of species j	$n_j / (n_N + n_j)$	–
z	Energy ratio	$k_B T_e / E_s$	–
Particle velocities and energies			
ϵ	Average electron temperature	$3k_B T_e / 2$	J
E_F	Fermi energy in electron gas	$\frac{\hbar^2}{2m} (3\pi^2 n)^{2/3}$	J
E_s	Mean ion energy	$E_+ + E_T = m_+ v_+^2 / 2$	J
E_T	Thermal ion energy	$m_+ v_T^2 / 2$	J
E_{UV}	UV photon energy	$E_{UV} = h\nu_{UV} = hc/\lambda_{UV}$	J
E_+	Kinetic ion energy	$m u_+^2 / 2$	J
M_T	Thermal ion Mach number	u_+ / v_T	–
\mathbf{u}_+	Ion drift velocity	$\mu_+ \mathbf{E}_{eff}$	m s^{-1}
u_B	Bohm velocity	$(k_B T_e / m_+)^{1/2}$	m s^{-1}
\mathbf{v}_{dr}	General drift velocity	$\mathbf{F} \times \mathbf{B} / q_j B^2$	m s^{-1}
\mathbf{v}_E	$\mathbf{E} \times \mathbf{B}$ drift velocity	$\mathbf{E} \times \mathbf{B} / B^2$	m s^{-1}
\mathbf{v}_P	Pressure gradient drift velocity	$\nabla P \times \mathbf{B} / en B^2$	m s^{-1}
v_{ph}	Phase velocity of dust acoustic wave	$(k_B T_+ n_D Z_D^2 / m_D n_+)^{1/2}$	m s^{-1}
v_+	Mean ion velocity	–	m s^{-1}

Short**Full**

Acronyms

AC	Alternating Current
CCD	Charge-Coupled Device
DC	Direct Current
DPX	Dusty Plasma eXperiment
ITER	the International Thermonuclear Experimental Reactor
Nd-YAG	Neodymium doped Yttrium Aluminium Garnet
OML	Orbital Motion Limited theory
Op-Amp	Operational Amplifier
PIC/MC	Particle-In-Cell plus Monte Carlo
PIV	Particle Image Velocimetry
PKE	Plasma Kristall Experiment
RF	Radio Frequency
YSO	Young Stellar Object

Contents

1	Introduction	1
1.1	Plasma	1
1.2	Dusty plasma	4
1.3	Previous work, Contribution of this thesis	7
1.4	Outline thesis	8
1.5	Publications related to this thesis	9
2	Theory of dusty plasma	15
2.1	Creating a plasma	15
2.1.1	DC discharge	17
2.1.2	Capacitively coupled RF discharge	18
2.2	Properties of dusty plasma	20
2.2.1	Quasi-neutrality	20
2.2.2	Quasi-neutrality with dust	22
2.2.3	Screening	22
2.2.4	Particle charging	25
2.3	Forces acting on dust particles	33
2.3.1	Electrostatic force	33
2.3.2	Gravity	34
2.3.3	Ion drag force	34
2.3.4	Neutral drag force	38
2.3.5	Thermophoretic force	39
2.3.6	Mutual Coulomb interaction	40
2.3.7	Summary	41
2.3.8	Void formation	41
2.4	Simulation models	41
2.4.1	Fluid model	41
2.4.2	Particle-in-Cell plus Monte Carlo	44

1. Introduction

1.1 Plasma

On Earth, we are most often confronted with solids, fluids and gases. As an example, at atmospheric pressure and at room temperature, water is in what is called the liquid state. Cooling it below the freezing point turns it into a solid, while it turns into a gas when heated above the boiling point. It is clear that the temperature of the water (or the amount of energy that is put into it) determines the state it is in.

Heating the water increases the average amount of kinetic energy per molecule. Therefore, the molecules move faster and faster. When the gas is hot enough, collisions between molecules make them fall apart into separate atoms, or groups of atoms. Heating the gas even more results in collisions between atoms in which electrons, bound to the core of the atom, gain so much energy that they overcome this bond and escape, leaving a positively charged ion behind. This results in a mixture of negatively charged electrons, the positively charged ions, and of course neutral atoms which have not yet experienced such a violent collision.

We call this soup of particles *plasma*, which is sometimes referred to as the fourth state of matter (after the three aforementioned states), even though there is no sudden transition from the gas into the plasma state. It now also becomes clear why we are so unfamiliar with the concept of plasma in our every day life; electrons are tightly bound to atoms and it takes a lot of energy to release them. Therefore, high temperatures are involved in the creation of a plasma at atmospheric pressures, temperatures we fortunately do not often experience.

In space, plasmas occur much more frequently. In fact, it is estimated that more than 90% of the (visible) universe is in the plasma state. This means that *plasma is the most common state of matter in the (visible) universe* [1]. Stars (and planets) are continuously born from huge, but very cold plasmas called *molecular clouds*. These, in a way, are enormous recycling factories in which the remnants of stars which have since long ceased to exist, are again used to form new stars.

Stars (like the Sun) are made of very hot plasma. In this plasma environment the internal engine of the stars burns through the process of fusion. In this process two ions are accelerated to energies high enough to overcome the repelling electrostatic force between them, allowing them to come so close together that the nuclear force binds them together to form a heavier element. Due to the binding energy, the separate ions are heavier than the new element formed by the ions fused together. This mass-deficit corresponds to a gain in energy, which is released in the form of energetic γ -photons. After more than 10^5 years of being

absorbed and re-emitted, do these photons finally escape the Sun at a wavelength roughly between the UV and the infrared [2]. Hot particles near the surface are also able to escape away from the star, resulting in a constant stream of energetic particles pouring into space, called the *stellar wind*. This stellar wind fills the interstellar space, resulting in yet another, albeit a very tenuous, plasma.

The interaction of emitted photons and the stellar wind with objects orbiting stars results in even more plasmas. The bright *tails of comets* close to the Sun consist of gas evaporating from the surface of the cometary core, ionized by the intense solar radiation, see the example in figure 1.1. The glow of the *polar lights* is emitted by plasma, formed by highly energetic particles originating from the solar wind interacting with molecules in the Earth's atmosphere. These solar wind particles are guided there by the helio- and geomagnetic fields, together forming the magnetosphere.



Figure 1.1: The Hale-Bopp comet close to the Sun. Two tails are visible: the tenuous plasma tail on the left, glowing blue in this picture, and the bright white dust tail on the right. The difference in angle is due to the light pressure induced by photons emitted by the Sun. The heavy dust particles are not influenced much by this light pressure and therefore the dust tail is directed along the orbital path of the comet. The plasma tail always points directly away from the Sun. *Courtesy of Wei-Hao Wang, IFA*

The upper part of the atmosphere is called the *ionosphere* and is the result

of ionization of oxygen (O_2), nitrogen (N_2) and nitric oxide (NO) by ultraviolet (UV) and soft Röntgen (X-ray) radiation from the Sun (during daytime) and by ionization through interactions between cosmic ray particles and the air [3, 4]. The free electrons present in the ionospheric plasma reflect electromagnetic waves, a property well known for its use in long-range radio communication.

In the atmosphere, charging of water vapor inside clouds can lead to electric fields strong enough to guide electric currents to run through the insulating air. Even though there are several types of these discharges, the most common one, usually visible between the clouds, or between the clouds and the ground, is called *lightning*. The light emitted by the lightning is due to the heating of the air by the current, resulting in a hot, but very short-lived plasma.

Ever since techniques both to pump gases in a confined volume to low pressures, as well as to apply large electric potentials to metallic surfaces were invented, plasmas are widely present in laboratories and in industry, introducing plasma to more human scales. Currently, one of the biggest efforts in plasma physics is to harness the power of fusion in order to find a new way to produce energy in large amounts. A promising concept uses a hot plasma confined by strong magnetic fields in a device called a Tokamak. In this device, a plasma is heated to 150 million degrees Celsius. The magnetic fields are used to keep the hot plasma away from the walls, which ensures that the plasma remains hot enough for hydrogen to fuse into helium. The field of fusion research, or high temperature plasma physics, has shown such a strong progress that in 2015 the world's first burning plasma experiment, ITER, will become operational. This device is being constructed in Cadarache, in the south of France, and will produce more energy than is needed to sustain the fusion process, during pulses of several minutes. ITER allows fusion science to progress towards a commercially viable fusion device within the next 50 years, or so. Therefore, fusion is a promising source of energy, which could help solve the energy problem.

Many everyday appliances involve plasmas at more moderate temperatures¹. These include gas discharge lighting, such as neon lighting used for commercial purposes, and fluorescent lighting, such as compact fluorescence light sources (CFL's), which have a higher efficiency than the traditional incandescent light sources. Modern display techniques include plasma screens, in which small plasma discharges are used to excite a phosphor layer, which then emits light. Organic light-emitting diodes (or OLEDs) can be used as light sources or as display panels, and are partly produced with the help of plasma assisted chemical vapor deposition [5].

¹Many of the plasmas discussed in this thesis are at temperatures of a few electronvolts (eV). One electronvolt corresponds to a temperature of $e/k_B = 11604.5$ K, or roughly twice the temperature of the visible surface of the Sun.

In modern microchip industry small structures are build with the help of plasma [6]. Next generation microchips require bright sources of extreme ultraviolet (EUV) photons. The idea is to use plasmas to create these photons [7]. Solar cells are build using plasma deposition techniques and surfaces can be treated with plasmas, for instance to change the wettability or the surface roughness of artificial limbs or dental implants [8]. Plasma sources are even used for direct sterilization of contaminated surfaces or for the treatment of cancer cells [9].

In many of the above processes, chemically active gases are used to make plasmas or are introduced into plasma. Through chemical nucleation, small particles, consisting of several hundreds of atoms, form in these plasmas. Coagulation between these particles results in larger particles with a size up to 100 nm. Finally, attachment of radicals on their surface leads to micron sized particles [10]. In fusion plasmas, violent plasma-wall interactions can lead to the introduction of very large particles in the plasma volume, up to several millimeters in size, which are often redeposited at different locations, as shown in figure 1.2 taken from [11]. Plasma containing dust particles is usually referred to as dusty plasma, but is also known as 'colloidal' or 'complex' plasma.

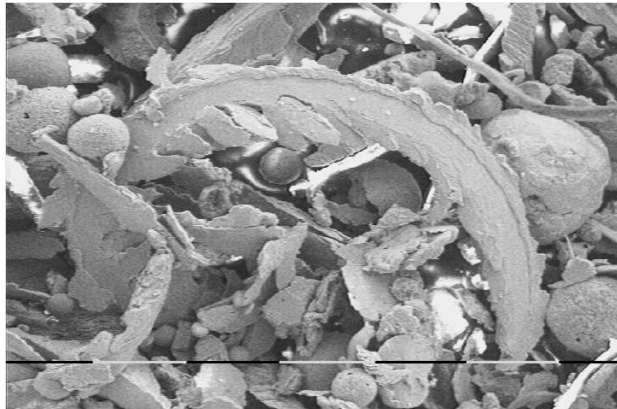


Figure 1.2: Dust found in the divertor region of the TEXTOR fusion experiment. The black and white line indicates intervals of 0.1 mm. Figure adapted from [11].

1.2 Dusty plasma

The formation and presence of dust in plasma discharges has been widely investigated both experimentally, e.g. [12], as well as numerically [13, 14]. In some cases, it was found that the presence of dust particles had a positive influence on

the efficiency of solar cells [15, 16], whereas small "killer particles" can destroy microchips during their plasma enhanced fabrication [17].

In any case, dust particles collect electrons and ions from the plasma, which means they become electrically charged. In laboratory plasmas, the higher mobility of the electrons as compared to the ions leads to a negative dust charge. A micrometer sized dust particle can have a negative charge of several thousands of electron charges. This means that in laboratory plasmas, dust is confined inside plasma discharges by the electric field, since the outer parts of discharges also become negatively charged with respect to the bulk of the plasma.

Another important force acting on the dust particles results from the positive ions being collected and deflected by the negatively charged dust particles. Furthermore, dust particles will interact with each other through the mutual Coulomb interaction, which can result in the formation of several types of dust structures.

Since dust collects plasma, the presence of dust strongly influences the plasma properties, such as the plasma densities, potential, and the energy distribution functions of the plasma particles. This means that ways to control the formation of the dust, or ways to control the dust once it is formed, are desirable for an efficient use of plasmas in industry. Furthermore, magnetic fields are often used, as in magnetron sputtering devices or fusion devices. The role of magnetic fields must therefore be taken into account for many relevant dusty plasmas.

Dusty plasmas are also interesting from a more fundamental point of view. To understand the behavior of cometary tails, the rings around Saturn, or noctilucent clouds, one has to understand the charging properties of dust particles. The formation of stars, such as the Sun, also involves dusty plasma.

Stars are born from large atomic and molecular clouds, which fill up interstellar space. When these clouds are locally perturbed, for instance by a passing shock wave originating from a nearby supernova explosion, a small part of the cloud starts to collapse under the influence of gravity. During this collapse, the gas heats up due to internal friction, which increases the pressure that counters the collapse under the force of gravity. Unless there is an efficient heat-removal mechanism, the clouds will then stop collapsing.

Dust particles in the plasma are efficient radiators and will, at intermediate dust densities, remove the excess heat, allowing the molecular clouds to collapse further. During the later stages of star formation, the heat produced during collapse is actually needed to ignite the young star at the center of the cloud. Dust at higher densities can no longer emit the energy outwards, but actually keeps the heat inside the system. The pressure and temperature in the core of the collapsing molecular cloud keep building up, until ignition occurs. From then on, the fusion processes dictate the energy balance of the system, and a star is born [18, 19].

Once the star is ignited, the light pressure will remove most of what remains of the molecular cloud, until only a rotating disk of plasma and dust remains, an

example of which is shown in figure 1.3. It is believed that from the micron-sized dust particles in these disks, planets form through the coagulation of these particles to larger and larger objects [20, 21]. Indeed, recent experiments seem to support that idea [22, 23], while recent observations around young stellar objects prove the presence of both amorphous as well as crystalline dust around young stars [24, 25].

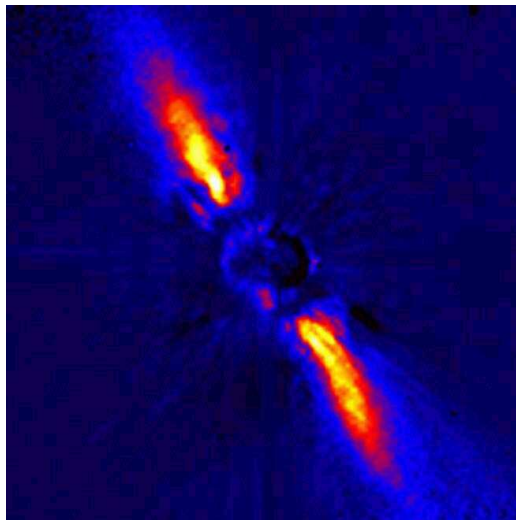


Figure 1.3: A coronagraphic picture of the dust disk around a nearby young star, β -Pictoris. The bright light from the young star has been blocked, using a coronagraph. The bright, yellow regions correspond to the disk of dust and gas orbiting the young star. *Courtesy of J. L. Beuzit et al., Grenoble Observatory, ESO*

How these dust particles coagulate on the short timescales required by cosmological theories, is still an unanswered question, especially since they should become negatively charged in the plasma around the young star. Jets and matter outflows observed in such objects are indications of the presence of strong magnetic fields, which might play an important role in the star and planet formation processes [26]. Energetic particles from space, as well as strong UV radiation from the central young star might interact with the dust, removing electrons from the dust. This might increase the probability of dust coagulation.

It is clear from the above that a good understanding of dusty plasmas is required to optimize many industrial applications of plasma, but also to fully comprehend the process of star and planet formation. This better understanding includes an understanding of the role of magnetic fields in dusty plasma, the interaction between the plasma and the dust, the forces acting on the dust, and of

course the effect of dust on the plasma parameters, as well as an understanding of the charging of dust particles through different charging processes.

The behavior of dusty plasmas, especially in the presence of magnetic fields and UV radiation, has been investigated with different numerical models, but also in an experimental study of magnetized dusty plasma discharges. By presenting the results of these studies, this thesis intends to bring a better insight into this behavior, both from a fundamental, as well as a practical point of view.

1.3 Previous work, Contribution of this thesis

In the past, numerical codes for the simulation of RF discharges were developed. A fluid model was used to simulate the deposition of silicon for the fabrication of solar cells in silane discharges [27, 28]. This model was then expanded to include the dust component coupled to the plasma solutions and was used to simulate results from microgravity experiments [29].

This model includes the dust charging problem, recombination of plasma particles on the dust particles and the corresponding heating of the dust. From the interaction between the plasma and the dust, the forces acting on the dust particles are calculated and from these forces the dust transport through the plasma, where the problem of the huge difference in transport time of the plasma particles (as short as nanoseconds for electrons) and the dust particles (as long as seconds for micrometer sized dust particles) is dealt with.

We have extended this code with a more sophisticated form for the interaction between ions and dust particles, including analytical forms for calculating this force in the presence of significant ion flow speeds and ion-neutral collisions, and we added the effect of charge exchange collisions on the charging of dust particles. We also computed the effect of a homogeneous magnetic field on the transport of plasma particles perpendicular to this field, and the corresponding effect on the dust transport through the plasma. Finally, we modelled the effect of a homogeneous flux of UV ions on the charging of dust particles and investigated the effect on dust transport and the void formation.

In fluid codes, time and space averaged plasma properties are calculated by solving the balance equations for the plasma particle densities and the energy density, often by using the so called *drift-diffusion approximation*. Another technique, called Particle-In-Cell plus Monte Carlo (PIC/MC), follows a large collection of super particles in real time and solves the equation of motion for every super particle. The electric field, which moves the particles, is found by solving the Poisson equation, which gives the electrostatic potential calculated from the charge density, which is interpolated from the positions of the super particles. Collisions between plasma particles and background neutrals are included in the

Monte Carlo scheme. They do not collide with or among each other however, see e.g. [30].

The latter type of models allows to examine the physics of plasmas on very short time scales and very small length scales. Such a model in one dimension was previously developed, including collisions between the plasma particles and a static dust distribution, where the dust charging was solved [31]. We have extended this model with an intense UV flux and the effect of this flux on the dust charge as well as the ionization of the background gas by this UV flux, including the effect of optical depth.

1.4 Outline thesis

The focus of this thesis is on the interaction between plasma and dust particles immersed in this plasma, and on the effect of magnetic fields and UV radiation on dusty plasmas.

Chapter 2 deals with the general theory of dusty plasma, together with a short description of the fluid code and Particle-In-Cell/Monte Carlo code used to obtain the results of this thesis.

Chapter 3 presents modelling results for the fluid code extended with an axial magnetic field, especially focussing on the effect of the magnetic field on the transport of the dust through the experiment and the formation of the so called *void* structure.

Chapter 4 deals with experimental measurements on the response of complex plasmas in a DC discharge with an applied magnetic field. It explains the different experimental techniques used to characterize the dusty plasma, as well as the secondary effect of applying a magnetic field when an electric field is present, namely $\mathbf{E} \times \mathbf{B}$ drifts of plasma particles and induced dust drift.

Chapter 5 presents results of the fluid code on the interaction between ions and dust particles. It describes the specific problem of non-linear scattering of ions in the potential around dust particles, together with the effect of ion flow speed and ion-neutral collisions on the transfer of momentum on the dust, as well as on the dust charging, and how these effects have been implemented in the fluid code.

Chapter 6 shows the effect of the dust on the plasma parameters, especially looking at the effect on the electron density and temperature. Special attention is given to where the energy required for the ionization inside the dust free void originates from and what role the electrons play in the process of void formation.

Chapter 7 shows results from the PIC/MC code on the effect of UV radiation on the dusty plasmas modelled. The chapter focuses on the reduction of dust charge by the effect of photo-detachment, while at the same time looking at the ef-

fect of the photo-detached electrons on the discharge. It also shows computations on the dynamic response of dusty plasma to a short pulse of UV light.

A general overview and the conclusions of this thesis are then presented, as well as recommendations for future research.

1.5 Publications related to this thesis

Refereed journal articles related to chapters of this thesis

- V. Land, W. J. Goedheer, and M. R. Akdim, *Dust transport in a magnetized radio-frequency discharge under microgravity conditions*, Physical Review E, Vol **72**, 046403, (2005) Chapter 3
- V. Land, and W. J. Goedheer, *Effect of large-angle scattering, ion flow speed and ion-neutral collisions on dust transport under microgravity conditions*, New Journal of Physics, Vol **8**, 8 (2006) Chapter 5
- V. Land, and W. J. Goedheer, *The plasma inside a dust free void: Hotter, denser, or both?*, New Journal of Physics, Vol **9**, 246 (2007) Chapter 6
- V. Land, and W. J. Goedheer, *Manipulating dust charge using ultraviolet light in complex plasma*, IEEE Trans. Plasma Sci., Vol **35**, Issue 2, Part 2, 280-285 (2007) Chapter 7

Articles not related to this thesis

- W. J. Goedheer, M. R. Akdim, and V. Land, *Transport of dust in low-pressure RF discharges*, High Temperature Material Processes, Vol. **8**, P. 139-148 (2004)
- W. J. Goedheer, and V. Land, *Shrinking voids and Yukawa-balls in RF-discharges under micro-gravity*, Submitted to Physical Review Letters, 2007
- V. Land, and W. J. Goedheer, *The role of self-organization in dusty plasmas under micro-gravity*, in preparation

Oral contributions to various international workshops and conferences

The contributions below marked with * were accompanied by a 4-paper conference proceeding.

1. * V. Land, W. J. Goedheer, and M. R. Akdim, *Transport of dust in plasmas with magnetic field and UV-radiation*, 31st European Physical Society Conference on Plasma Physics, London, United Kingdom, June 28 - July 2 (2004)
2. V. Land and W. J. Goedheer, *Dust transport and azimuthal flow in dusty magnetized RF discharge*, 7th Workshop on the Exploration of Low Temperature Plasma Physics, Kerkrade, The Netherlands, November 25-26 (2004)
3. V. Land, W. J. Goedheer, *Dusty plasmas in the presence of ultra-violet light*, 18th NNV/CPS Symposium on Plasma Physics and Radiation Technology, Lunteren, the Netherlands, March 22-23 (2006)
4. V. Land, W. J. Goedheer, *Manipulating dust in plasma with UV, Particle-In-Cell plus Monte Carlo simulations*, 11th Workshop on the Physics of Dusty Plasmas, Williamsburg, VA, United States of America, June 28 - July 2 (2006)
5. V. Land, W. J. Goedheer, *Can we Use UV light to control dust charging? An investigation using Particle-In-Cell/Monte Carlo simulations*, Diagnostics and Simulation of Dusty Plasmas, Kiel, Germany, September 13 - 15 (2006)
6. W. J. Goedheer, V. Land, M. R. Akdim, *Simulation of dust voids*, Diagnostics and Simulation of Dusty Plasmas, Kiel, Germany, September 13 - 15 (2006)
7. * V. Land, W. J. Goedheer, *Electrons in a dust free void: "Hotter or denser?"*, 34th European Physical Society Conference on Plasma Physics, Warsaw, Poland, July 2-6 (2007)

Poster contributions to various international workshops and conferences

1. V. Land, W. J. Goedheer, and M. R. Akdim, *Toward the understanding of Astronomical Dusty Plasmas: Modelling of asymmetric and magnetized plasmas*, 16th NNV/CPS Symposium on Plasma Physics and Radiation Technology, Lunteren, the Netherlands, March 16-17 (2004)
2. * V. Land, and W. J. Goedheer, *Charged dust particles in a RF and UV-driven plasma*, 4th International Conference on the Physics of Dusty Plasmas, Orléans, France, June 13 - 17 (2005)
3. * V. Land, E. Thomas, Jr., and Jeremaiah Williams, *Dust transport and force equilibria in magnetized dusty DC discharges*, 4th International Conference on the Physics of Dusty Plasmas, Orléans, France, June 13 - 17 (2005)

4. * V. Land, E. Thomas, Jr., and Jeremaiah Williams, *Dust transport and force equilibria in magnetized dusty DC discharges*, 47th Annual Meeting of the Division of Plasma Physics, Denver, CO, United States of America, October 24 - 28 (2005)
5. * W. J. Goedheer, M. R. Akdim, and V. Land, *Void formation and dust cloud structure in (a)symmetric RF discharge*, 4th International Conference on the Physics of Dusty Plasmas, Orléans, France, June 13 - 17 (2005)
6. V. Land, W. J. Goedheer, *MC-PIC modelling of multiple dust species in plasma with UV radiation*, 8th Workshop on the Exploration of Low Temperature Plasma Physics, Kerkrade, The Netherlands, November 24-25 (2005)
7. V. Land, W. J. Goedheer, *Ion-dust interactions in dusty plasmas*, 18th NNV/CPS Symposium on Plasma Physics and Radiation Technology, Lunteren, the Netherlands, March 21-22 (2006)
8. V. Land, W. J. Goedheer, *Dynamic response of dusty plasma to UV radiation*, 9th Workshop on the Exploration of Low Temperature Plasma Physics, Kerkrade, The Netherlands, November 23-24 (2006)
9. * V. Land, W. J. Goedheer, *Dynamic response of dusty plasma*, 34th European Physical Society Conference on Plasma Physics, Warsaw, Poland, July 2-6 (2007)

Seminars

- *Ion drift in magnetized dusty discharge and induced dust flow*, Auburn University, Auburn, Al, United States of America, March 17 (2005)
- *Computing the complex, simulations of dusty plasmas*, Ruhr University Bochum, Bochum, Germany, November 16 (2006)
- *Creation and closing of dust free voids in dusty plasma*, University of Antwerp, Antwerp, Belgium, June 4 (2007)

References

- [1] J. P. Goedbloed, and S. Poedts, *Principles of Magnetohydrodynamics with applications to laboratory and astrophysical plasmas*, Cambridge University Press, Cambridge, (2004)
- [2] R. Mitalas, and K. R. Sills, *Astrophysical Journal* **401**, 759 (1992)
- [3] E. O. Hulburt, *Physical Review*, **53**, 344-351 (1938)
- [4] P. Meyer, E. N. Parker, and J. A. Simpson, *Physical Review* **104**, 3, 768-783 (1956)
- [5] H.-K. Kim, M. S. Kim, J.-W. Kang, J.-J. Kim, M.-S. Yi, *Appl. Phys. Lett.* **90**, 013502 (2007)
- [6] S. Tachi, *J. Vac. Sci. Technol. A* **21**, S131 (2003)
- [7] A. P. Shevelko, L. A. Shmaenok, S. S. Churilov, R. K. F. J. Bastiaansen, and F. Bijkerk, *Phys. Scr.* **57**, 276-282 (1998)
- [8] M. A. M. Silva, A. E. Martinelli, C. Alves Jr., R. M. Nascimento, M. P. Távora, and C. D. Vilar, *Surface & Coatings Technol.* **200**, 2618-2626 (2006)
- [9] E. Stoffels, A. J. Flikweert, W. W. Stoffels, and G. M. W. Kroesen, *Plasma Sources Sci. Technol.* **11**, 383-388 (2002)
- [10] K. De Bleecker, A. Bogaerts, and W. Goedheer, *New J. Phys.* **8**, 178 (2006)
- [11] J. Winter, *Plasma Phys. Control. Fusion*, **40**, 1201 (1998).
- [12] W. W. Stoffels and E. Stoffels, *Trends Vac. Sci. Technol.* **4**, 1 (2001)
- [13] K. De Bleecker, A. Bogaerts, R. Gijbels, and W. Goedheer, *Phys. Rev. E* **69**, 056409 (2004)
- [14] K. De Bleecker, A. Bogaerts, and W. Goedheer, *Phys. Rev. E* **70**, 056407 (2004)

-
- [15] C. Longeaud, J. P. Kleider, P. Roca i Cabarrocas, S. Hamma, R. Meaudre, and M. Meaudre, *J. Non-Cryst. Solids* **227-230**, 96 (1998)
- [16] M. Meaudre, R. Meaudre, R. Butté, and S. Vignoli, *J. Appl. Phys.* **86**, 946 (1999)
- [17] G. S. Selwyn, J. Singh, and R. S. Bennett, *J. Vac. Sci. Technol. A* **7**, 2758 (1989)
- [18] F. H. Shu, In: *The Milky Way Galaxy*, Proceedings of the 106th Symposium Groningen, The Netherlands, P. 561-566 (1985)
- [19] R. Chini, E. Krügel, and E. Kreysa, *A&A* **167**, 315-324 (1986)
- [20] S. J. Weidenschilling, and J. N. Cuzzi, *Protostars and Planets III*, 1031, 1993
- [21] S. V. W. Beckwith, T. Henning, and Y. Nakagawa, *Protostars and Planets IV*, 533 (2000)
- [22] T. Poppe, J. Blum, and T. Henning, *Astr. J.* **533**, 454-471, (2000)
- [23] T. Poppe, J. Blum, and T. Henning, *Astr. J.* **533**, 472-480, (2000)
- [24] Y. K. Okamoto *et al.*, *Nature (London)*, **431**, 660 (2004)
- [25] C. M. Telesco *et al.*, *Nature (London)*, **433**, 133 (2005)
- [26] G. T. Birk, *Astron. Astrophys.* **330**, 1070 (1998)
- [27] J. D. P. Passchier, *Numerical fluid models for RF discharges*, Ph.D. Thesis, University Utrecht, The Netherlands, 1994
- [28] G. J. Nienhuis, *Plasma models for silicon deposition*, Ph.D. Thesis, University Utrecht, The Netherlands, 1998
- [29] M. R. Akdim, *Modelling of Complex Plasmas*, Ph.D. Thesis, University Utrecht, The Netherlands, 2003
- [30] C. K. Birdsall, *IEEE Trans. Plasma Sci.*, **19** (1991), 65-85
- [31] W. J. Goedheer, Y. I. Chutov, *IEEE Trans. Plasma Sci.*, **32** (2004) 551-554

2. Theory of dusty plasma

As was already mentioned in the introduction, plasma is a very common state of matter in the universe. In our everyday life, we are not often confronted with it though. This needs some more explanation about how plasmas actually form and which techniques are used in laboratories all over the world to make plasmas.

In order to appreciate statements about dusty plasmas, a basic understanding of several plasma properties needs to be provided. These properties include so called quasi-neutrality, the screening of charges by plasma, a knowledge about how dust particles charge up in a plasma, and which forces will then act upon them.

This chapter tries to do all that, explains the phenomenon of void formation in dusty plasmas under micro-gravity, and gives an overview of the numerical methods with which the results presented in this thesis are obtained.

2.1 Creating a plasma

A plasma consists of a mixture of charged particles, electrons and ions, and neutrals. The ratio of ions (for instance Ar^+) over the total particle density, $x = n_+/(n_N + n_+)$ (in this example then $x_{\text{Ar}^+} = \text{Ar}^+ / (\text{Ar} + \text{Ar}^+)$) is called the *ionization fraction* and differs for different types of plasmas. In a fusion experiment it will be much higher than in a gas discharge light source. For a plasma where locally the volume production balances the volume losses, for instance electron impact ionization and three-particle recombination, the ionization fraction can be described by the Saha equation [1]. Assuming that all the components of the plasma have the same temperature ($T_N = T_+ = T_e \equiv T$), i.e. assuming that the plasma is in *thermal equilibrium*, this equation becomes

$$\left(\frac{x}{1-x}\right) n_e = \frac{2U_{r+1}}{U_r} \left(\frac{2\pi m_e k_B T}{h^2}\right)^{3/2} e^{-\chi_r/k_B T}, \quad (2.1)$$

where $U_y \equiv \sum_s g_{y,s} e^{-\chi_{y,s}/k_B T}$ is the partition function of the ionized state y which has s degenerate states with statistical weight g_s , χ_r is the ionization energy needed to go from state $r - 1$ to r , typically an energy of several eV, and the term $(\dots)^{3/2}$ is the cube of the reciprocal of the de Broglie wavelength.

For gases where only one ionization level is important, such as atomic hydrogen, the electron density can be expressed in terms of the total pressure, $n_e k_B T = n_{tot} k_B T (x/(x+1)) = P_{tot} (x/(x+1))$, where $n_{tot} = n_e + n_+ + n_N$. This leads to the following expression for the ionization fraction, x ,

$$\left(\frac{x^2}{1-x^2}\right) = \frac{2U_{r+1}}{U_r} \left(\frac{2\pi m_e k_B T}{h^2}\right)^{3/2} \frac{k_B T}{P_{tot}} e^{-\chi_r/k_B T}. \quad (2.2)$$

We can see that for increasing pressure, a higher temperature is needed to achieve the same ionization fraction. This is due to the increasing chance of recombination at higher pressures. We also see that at fixed pressure, the ionization degree increases for increasing temperature, which is due to the fact that on average the collisions become more and more energetic. Filling in the numbers and using $U_r = 2$ and $U_{r+1} = 1$, we find for partly ionized gases ($n_+ < n_N$) [2],

$$x \sim \frac{n_+}{n_N} \approx 2.4 \times 10^{21} \frac{T^{3/2}}{n_+} e^{-\chi_r/k_B T}. \quad (2.3)$$

From the above equation it is clear that very high equilibrium temperatures are needed to get even a modest ionization fraction, because of the exponential term. This is also the reason why we are not used to the plasma state on Earth; both the gas temperatures are too low, and the neutral gas pressures are too high.

In experiments, such as described in this thesis, the ionization fraction is very low ($x \leq 10^{-6}$), so that the energy transfer from the electrons to the ions and neutrals is insufficient to reach local equilibrium. On the contrary, electron impact ionization is balanced by (Bohm) losses to the walls, or, in the presence of dust, in combination with recombination of plasma on the dust particles. Both the ionization as well as the (Bohm) loss terms are described by the electron temperature, T_e , but of course, the ionization is an exponential function of the temperature, whereas the losses are proportional to the square root of the temperature. The recombination of the dust is somewhat more complicated, but can also be described by the electron temperature.

So, in low pressure experiments, the balance is not given by the Saha equation, but by a non-local balance between production and losses. This balance is dominated by the electron temperature. Due to the high electron mobility, electrons can be efficiently heated to several electronvolts by the use of electric fields, whereas the heavy particle temperature can be close to room temperature.

There are many different types of plasma devices, one of which is the so called *direct current glow discharge* (DC discharge). Such a device was used to obtain the results presented in chapter 4. It will also be described below. In such a device, one of the electrodes is biased negatively (called the cathode), whereas the other is grounded or biased positively, resulting in a stationary electric field, which accelerates the charged species.

Another type of discharge, discussed in chapters 3, 5, 6 and 7, is the *radio frequency discharge* (RF discharge). In this case, one or both of the electrodes is powered with a sinusoidal signal, usually at 13.56 MHz. In this thesis, all the RF

discharges are modelled with a RF frequency of 13.56 MHz. This frequency is too high for the heavy ions to respond to, so that only the electrons are effectively heated by the electric field providing the energy for electron impact ionization. For most of these experiments we have $x \leq 10^{-6}$. This also means that the dominant class of collisions is between charged plasma particles and neutrals, and not collisions between charged plasma particles.

2.1.1 DC discharge

The oldest form of plasma discharges consists of a straight closed cylinder pumped to low pressures. A gas is introduced in the cylinder, which has two conducting electrodes at both ends. A constant negative potential is then applied to one of the electrodes (the *cathode*). The other electrode (*anode*) can be positively biased, but here we restrict ourselves to a grounded anode.

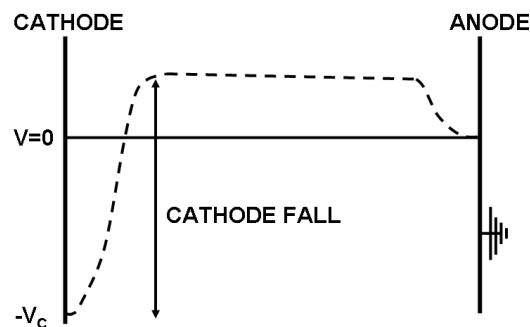


Figure 2.1: Schematic drawing of a simple DC discharge, with the dashed line showing the plasma potential. Sheaths build up, connecting the electrode potential to the bulk plasma potential. In these sheaths the electric field is large, accelerating electrons away from the electrodes. In the bulk, the electric field is very small. In the cathodic region, the largest potential difference occurs, called the "cathode fall". The true electric field in a DC discharge is much more complicated than shown here.

Due to random processes, like radiation from natural radio-active sources or energetic particles originating from cosmic rays, either atoms in the volume are ionized, or electrons are emitted from one of the electrodes. The electrons are

then accelerated in the electric field, away from the cathode, and gain energy. In inelastic processes they excite and ionize the background gas, resulting in more charged particles. The positive ions are accelerated towards the cathode and emit electrons on colliding with the cathode through the process of secondary electron emission. These electrons are again accelerated away from the cathode and a self-sustaining discharge is born.

At constant applied potential, a constant current will run, therefore such a discharge is called *direct current glow discharge*, or DC discharge. The main source of ionization in these discharges is due to the secondary electrons emitted from the cathode by ion-impact. This is called γ -ionization. A schematic picture of the most simple type of DC discharge is shown in figure 2.1.

2.1.2 Capacitively coupled RF discharge

When plasma is used to deposit layers, the electrode on which they are deposited is often rapidly covered with layers of insulating material, such as carbon containing compounds. In a DC discharge this electrode would therefore charge up until the discharge would extinguish. In order to overcome this problem, one can apply an alternating potential instead of a constant potential difference between the electrodes, so that both electrodes would become the anode and cathode alternately. This would allow the charge build up during half the cycle to be neutralized during the second half of the cycle. This is the principle behind *alternating current*, or AC discharges.

A special type of AC discharge is the *radio-frequency*, or RF discharge, which is powered by an alternating potential with a driving frequency in the radio-frequency range. One frequency often used (simply because it has been reserved for science research by international rules on radio-communication) is 13.56 MHz. This high frequency means that electrons can follow it instantaneously, but not the ions, since $\omega_{p,+} \lesssim \omega_{RF} \ll \omega_{p,e}$ for argon gas and plasma densities in the range of $n_e = n_+ \sim 10^{15} \text{ m}^{-3}$, with the plasma frequencies given by

$$\omega_{p,j} = \sqrt{\frac{n_j e^2}{m_j \epsilon_0}}. \quad (2.4)$$

This means that ions only see the (moderate) effective electric field, see equation 2.65, whereas electrons are accelerated in the (much stronger) instantaneous field. This also means that secondary electron emission is in general of minor importance for sustaining the discharge and that most of the excitation and ionization is due to fast electrons moving in the bulk of the discharge. This is called α -ionization.

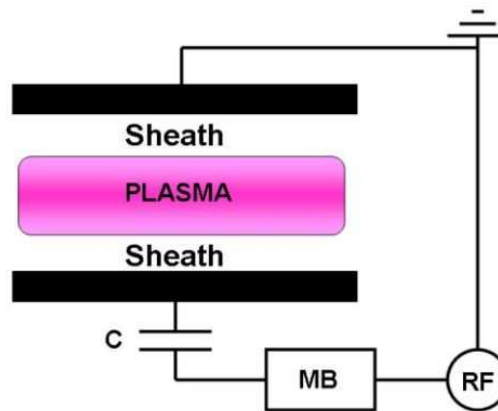


Figure 2.2: Schematic view of a typical RF discharge. The radio-frequency potential (RF) is coupled to the lower electrode through a matching box (MB), which allows the impedance to match the complex impedance of the plasma-sheath system (which could be represented by two capacitors in series with a resistor), and a blocking capacitor (C), which allows the build-up of a self-bias on the powered electrode.

Under certain circumstances (for instance when the size of both the electrodes is not equal), a self-bias can occur. During one half of the RF cycle, the amount of negative charge collected is then not neutralized during the second half of the cycle. This results in a negative charge on the electrode. This will continue until the extra negative charge repels enough of the extra electrons to the electrode so that the total electron and ion flux during one cycle becomes equal again. In this case, the negative bias can result in significant ion impact and then secondary electron emission can again become important, which can result in a significant γ contribution to the discharge. This process is referred to as the $\alpha - \gamma$ transition. In this thesis we will model symmetric *capacitively coupled* RF discharges, with negligible self-bias.

The term *capacitively coupled* refers to how the power is coupled to the plasma. In this case, the electrodes together with the sheaths act as a capacitor, as indicated in figure 2.2. It is also possible to couple the power by applying a time-varying magnetic field, which induces an electric field in the plasma. These discharges are called *inductively coupled* RF discharges. These are beyond the scope of this thesis. A broad overview of plasma discharges can be found in [3], whereas a numerical comparison between DC and RF discharges can be found in [4].

2.2 Properties of dusty plasma

Plasma has some very specific properties, but the presence of dust particles in the plasma alters these properties slightly. Looking from "far away" to an isolated plasma, one would not see any net charge of the plasma, since for every ionic charge created, a corresponding electron is created. This is called *quasi-neutrality*. This quasi-neutrality still holds when dust particles are introduced, even though these particles act like 'sponges', collecting electrons and ions, and *become charged*.

Micrometer sized particles can carry a considerable amount of charge on their surface. The fact that these large charges are not seen from far away means that the plasma organizes itself in such a way as to *screen* these charges from the surrounding plasma. Beyond a certain distance from the charge, which is called the *screening*, or *Debye length*, usually indicated by the symbol λ_D , the potential of the charged particle is no longer experienced by another charge¹, which also determines what "far away" means.

We now continue to define these notions mathematically, using simple physical considerations. We start with showing why a plasma is quasi-neutral except within the small length-scale of the Debye length.

2.2.1 Quasi-neutrality

To derive the condition for quasi-neutrality, we start with a neutral plasma with a homogeneous electron and ion background density, $n_{e0} = n_{+0} \equiv n_0$, at constant finite temperature throughout the volume of the plasma, i.e. $\nabla T_e = \nabla T_+ \equiv 0$.

When the ion density is disturbed locally, see figure 2.3, so that $n_+ \rightarrow n_0 + n_{+1}$, the induced net space charge accelerates the electrons towards the region of increased ion density. However, with this acceleration, an electron gradient builds up, which results in a pressure gradient acting in the opposite direction. Due to this restoring force, a net space charge remains within a small volume of the plasma.

The exact spatial extent of this charge separation can be derived from the force balance of the electrons after the perturbation,

$$\mathbf{F}_e = -en_e\mathbf{E} - \nabla P_e = 0. \quad (2.5)$$

Here, the electric field is due to the induced charge separation,

$$\nabla \cdot \mathbf{E} = \frac{\rho}{\epsilon_0} = \frac{e(n_{+1} - n_{e1})}{\epsilon_0}. \quad (2.6)$$

¹In fact, the Debye length is defined as the length where the strength of the potential around a charge is $1/e \approx 0.37$ times the potential at the position of the charge. So another charge would still experience some potential, but it will in principle be a small fraction of the particle potential.

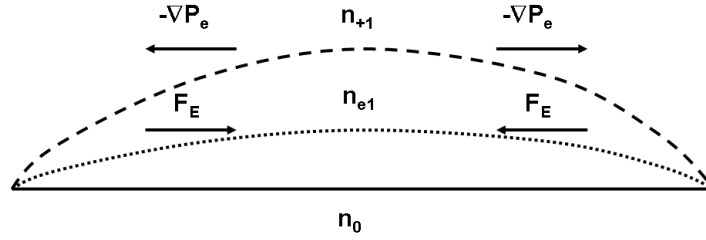


Figure 2.3: Illustration of a perturbation to a homogeneous plasma with initial plasma density n_0 . The ions are perturbed. The electrons respond to the positive space charge. This results in an electron pressure gradient which acts against the electric force. A net charge separation is the result.

Taking the divergence of equation 2.5, assuming the ideal gas law for the electrons, $P_e = n_e k_B T_e$, and assuming constant electron temperature during the perturbation, $T_{e1} = 0$, we find

$$-e(n_0 + n_{e1})(\nabla \cdot \mathbf{E}) - e\mathbf{E} \cdot \nabla(n_0 + n_{e1}) - k_B T_e \nabla^2(n_0 + n_{e1}) = 0. \quad (2.7)$$

Remembering that the initial plasma was homogeneous, and that \mathbf{E} only depends on perturbed quantities, we use equation 2.6 and linearize to get

$$\frac{-e^2 n_0}{k_B T_e \epsilon_0} (n_{+1} - n_{e1}) - \nabla^2 n_{e1} = 0. \quad (2.8)$$

Assuming that the perturbation of the background densities is periodic in space, $n_{e1} \propto \sin(x/L)$, with L the characteristic length of the perturbation, so that $\nabla^2 n_{e1} = -n_{e1}/L^2$, we end up with

$$-\frac{(n_{+1} - n_{e1})}{\lambda^2} + \frac{n_{e1}}{L^2} = 0. \quad (2.9)$$

Here $\lambda = (\epsilon_0 k_B T_e / e^2 n_0)^{1/2}$ is the (electron) Debye length. We find this way,

$$n_{e1} \left(\frac{\lambda^2}{L^2} + 1 \right) = n_{+1}. \quad (2.10)$$

We see that $n_{e1} \approx n_{+1}$ if $L \gg \lambda$, so that the plasma is always neutral over distances larger than the Debye length, as long as the amplitude of the perturbation is small so that the problem can be linearized. Therefore, the quasi-neutrality condition in the absence of dust, for a plasma with only singly charged positive ions and electrons, can be written as:

$$n_{+} - n_e = 0. \quad (2.11)$$

2.2.2 Quasi-neutrality with dust

Particles in a plasma collect ions and electrons and become charged. Due to the high electron mobility, this charge will in general be negative, as will be explained in section 2.2.4. Therefore, the dust charge must be taken into account when rewriting equation 2.11 for the case where dust is present. It therefore reads

$$n_+ - n_e - n_D \frac{Q_D}{e} = 0, \quad (2.12)$$

with $Q_D = eZ_D$ the dust charge.

Since in a dusty plasma the ions are no longer the heaviest species, the screening of charged dust particles will be some combination of screening by the mobile electrons and the less mobile positive ions in the plasma. We will derive the appropriate screening length in the next section.

2.2.3 Screening

We consider the response of plasma to a dust particle with surface charge $Q_D = eZ_D$, which is assumed to be known. To obtain this response we need to solve Poisson's equation,

$$\nabla \cdot \mathbf{E} = -\nabla^2 \phi(r) = \frac{\rho}{\epsilon_0} = -\frac{e}{\epsilon_0} (n_e - n_+). \quad (2.13)$$

We now make three approximations:

1. The energy distribution function of the ions and electrons are described by a Maxwellian distribution.
2. The dust charge is negative, so that the potential is repulsive for electrons and attractive for ions.
3. The disturbance caused by the charged particle is small, so that the potential energy of the ions and electrons is much smaller than their thermal energy.

The first approximation allows us to write the (collisionless) solution for the density of the electrons and ions around the dust particle, found from the Vlasov equation, by the Boltzmann distribution, $n_j \sim \exp(-E_{pot}/k_B T_j)$. The second approximation determines the sign in front of the exponential terms in this distribution, while the third allows us to linearize these exponential terms.

The potential energy for the electrons and ions respectively is $-e\phi(r)$ and $e\phi(r)$, so that we can write the densities as,

$$\begin{aligned} n_e(r) &= n_\infty \exp\left(\frac{e\phi(r)}{k_B T_e}\right), \\ n_+(r) &= n_\infty \exp\left(\frac{-e\phi(r)}{E_s}\right). \end{aligned} \quad (2.14)$$

Here, n_∞ is the density of charged plasma particles far away from the test charge in the potential $\phi(r)$ around the charged particle.

For the ions we use the mean energy rather than $k_B T_+$ since ions can have drifts close to the sheaths in front of the electrodes. The mean energy is given by [5] $E_s = m_+ v_+^2 / 2 = m_+ (u_+^2 + 8k_B T_+ / \pi m_+) / 2$. $u_+ = \mu_+ E_{eff}$ is the ion (with mobility μ_+) drift velocity in the effective electric field E_{eff} . We can rewrite this in terms of the thermal ion Mach number, $M_T = u_+ / v_T = u_+ / \sqrt{8k_B T_+ / \pi m_+}$, as $E_s = m_+ v_T^2 (1 + M_T^2) / 2$.

Linearizing equations 2.14, and using them in equation 2.13, we end up with,

$$\nabla^2 \phi(r) = \phi(r) \frac{e^2 n_\infty}{\epsilon_0} \left[\frac{1}{k_B T_e} + \frac{\pi}{4k_B T_+ (1 + M_T^2)} \right], \quad (2.15)$$

which becomes:

$$\nabla^2 \phi(r) = \frac{1}{\lambda_D^2} \phi(r). \quad (2.16)$$

In this equation $\lambda_D^{-2} = \frac{e^2 n_\infty}{\epsilon_0} \left[\frac{1}{k_B T_e} + \frac{\pi}{4k_B T_+ (1 + M_T^2)} \right] = \left[\lambda_e^{-2} + \frac{\pi}{4(1 + M_T^2)} \lambda_+^{-2} \right]$. λ_D is called the *linearized Debye length*.

The solution to the above equation in spherical coordinates is given by the Debye-Hückel potential:

$$\phi(r) = \frac{Q_D}{4\pi\epsilon_0 r} \exp\left(\frac{-r}{\lambda_D}\right). \quad (2.17)$$

Close to the test charge, the $1/r$ term dominates and we see that the potential is simply the Coulomb potential around the test charge. Further away, the $\exp(-r/\lambda_D)$ term dominates and the potential falls off more rapidly, due to the screening of the test charge by the plasma.

One approximation often made is to write the above solution as:

$$\begin{aligned} \phi(r) &= \frac{Q_D}{4\pi\epsilon_0 r}, \quad \forall r \leq \lambda_D, \\ &= 0, \quad \forall r > \lambda_D. \end{aligned} \quad (2.18)$$

This is also the reason why sometimes it is said that; "charged particles do not 'feel' each other, when they are farther apart than the Debye length", but technically speaking this is not so.

An important assumption in this derivation is that the perturbation of quasi-neutrality by the test charge is small. This is not so when $e\phi(r)/k_B T_{e,+} \gtrsim 1$. In this case the linearization of the exponent is no longer valid. Making the assumption that this happens close to the test charge, we then have $\phi(r) = Q_D/4\pi\epsilon_0 r$. So the radius for which this deviation from linearity happens, is then given by:

$$r_{max} \equiv 2\rho_{0,e,+} = \frac{eQ_D}{4\pi\epsilon_0 k_B T_{e,+}}. \quad (2.19)$$

Since $T_e \gg T_+$, the largest radius applies to the ions. The above radius, ρ_0 , is referred to as the "Coulomb radius" and it defines the radius within which screening is a non-linear problem. Writing the ion Coulomb radius, using the ion Debye length, we find:

$$\rho_{0,+} = \frac{Z_D}{8\pi n_\infty \lambda_+^2}. \quad (2.20)$$

Making an estimate of the different sizes in a typical dust free plasma with $Z_D = q_+ \sim 1$ at room temperature and with a density of $n_\infty = 10^{15} \text{ m}^{-3}$, we find;

$$\rho_0 \propto \frac{\Delta^3}{\lambda_+^2} < \Delta < \lambda_+, \quad (2.21)$$

where we have written $n_\infty \propto \Delta^{-3}$, with Δ the inter-particle distance. For such a dust free plasma, screening of an ion by the surrounding plasma is always a linear problem.

For a dust particle immersed in a plasma, $Z_D \gg 1$. This means that the Coulomb-radius can be much bigger than the average distance between the ions, so that there are always some ions inside the volume where the screening is non-linear. This happens when

$$\rho_0 > \Delta \leftrightarrow |Z_D| > \frac{\lambda_+^2}{\Delta^2}. \quad (2.22)$$

It is of course also possible that the region of non-linearity extends *beyond the Debye length*. In that case, the screening by *all* the ions will be non-linear. This happens when

$$\rho_0 > \lambda_+ \leftrightarrow |Z_D| > \frac{\lambda_+^3}{\Delta^3}. \quad (2.23)$$

Equation (2.22) is fulfilled for $|Z_D| \gtrsim 75$, whereas equation (2.23) is fulfilled for $|Z_D| \gtrsim 620$ for the plasma parameters mentioned. Figure 2.4 illustrates this.

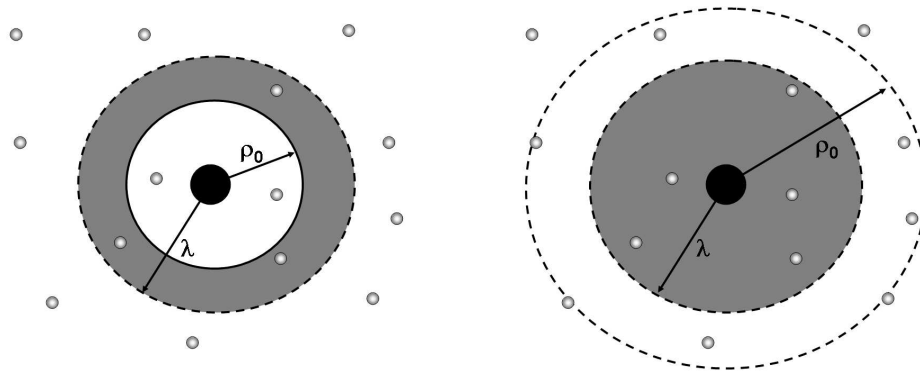


Figure 2.4: **Left:** The Coulomb radius is smaller than the screening length, but is bigger than the average distance between ions, so that some of the ions screening the dust particle are in the non-linear regime.

Right: The Coulomb radius is bigger than both the average distance between the ions, *as well as* the screening length. This means that all the ions that are screening the dust particle are in the non-linear regime, resulting in a larger scattering cross section.

Micrometer sized dust particles can carry several thousands of electron charges. This means that the screening of these particles by ions at room temperature (which is important in the bulk of the discharge, away from the sheaths), is a strongly non-linear problem. A description of this problem in fluid calculations of a dusty plasma is presented in chapter 5 in which a central role will be played by the ratio of the Coulomb radius over the Debye length,

$$\beta(v) = \frac{\rho_0(v)}{\lambda_D(v)}. \quad (2.24)$$

2.2.4 Particle charging

In the above discussion of the screening of dust particles, the surface charge was assumed to be known. In typical laboratory dusty plasmas, collection of charged plasma particles by the dust particles is the dominant charging process. Because of the low mass of the electrons with respect to the ions, the dust surface charge becomes negative, unless there are other important charging processes. The basic classical charging theory follows the trajectories of particles in the potential around the dust particle. This theory is called *Orbital Motion Limited* theory.

Orbital Motion Limited theory (OML)

The ion-collection cross section of a negatively charged dust particle will be bigger than the geometrical surface, since the ions are attracted by the particle. Consider an ion which passes at the dust particle surface with zero radial velocity, as shown in figure 2.5 (it either "just passes", or is "exactly captured").

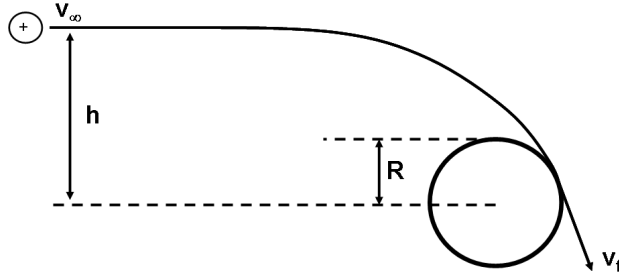


Figure 2.5: An ion comes with velocity v_∞ from the plasma with impact parameter h and is attracted by a negatively charged dust particle with radius R . When it passes the dust particle exactly at the surface, it has velocity v_f , which is tangential to this surface.

Assuming that the potential energy of the particle far away is zero, energy conservation says,

$$E = \frac{1}{2}m_+v_\infty^2 = \frac{1}{2}m_+v_f^2 + e\phi_D, \quad (2.25)$$

where ϕ_D is the dust particle surface potential. At the same time, conservation of angular momentum results in,

$$L_\infty = m_+v_\infty h = L_f = m_+v_f R. \quad (2.26)$$

Solving for v_f from equation 2.26, and substituting in equation 2.25, gives the impact parameter h ,

$$h = R\sqrt{1 - \frac{e\phi_D}{E}}, \quad (2.27)$$

This corresponds to an initial angular momentum of

$$L_\infty = L_{max} = m_+v_\infty h = m_+v_\infty R\sqrt{1 - \frac{e\phi_D}{E}}, \quad (2.28)$$

where we have labelled it as L_{max} , since we assume that any ion approaching with more angular momentum will miss the dust particle, whereas any ion with less or equal angular momentum will be collected.

This way, the ion current contribution is given by [6]:

$$dI = -ef(v)u(r)d^3v \quad L \leq L_{max}. \quad (2.29)$$

Integrating over the sphere and over velocity space, gives for the total collected ion current,

$$I_+ = 4\pi r^2 \int_{L \leq L_{max}} ef(v)u(r)d^3v. \quad (2.30)$$

$f(v)$ is the ion velocity distribution function, and $u(r)$ is the radial velocity at position $r > R$, positive being radially outwards. Assuming that the ion distribution is a Maxwellian², but using the mean energy, rather than the thermal energy, and using equation 2.25, and 2.26 to find

$u(r) = \sqrt{2(E - eV(r))/m_+ - L^2(r)/m_+^2 r^2}$, and changing variables, we find for the ion collection current:

$$I_+ = 4\pi R^2 en_\infty \sqrt{\frac{E_s}{2m_+}} \left(1 - \frac{e\phi_D}{E_s}\right) \approx 4\pi R^2 en_\infty \sqrt{\frac{E_s}{2m_+}} \frac{e|\phi_D|}{E_s}, \quad (2.31)$$

where n_∞ is the ion density far away from the dust particle.

The derivation for the electron current is much more straight-forward [7]. Simply assuming that the density of electrons in the repelling potential around the dust particle is given by the Boltzmann distribution, and integrating over velocity space, we find for the electron current, assuming quasi-neutrality far away from the dust particle,

$$I_e = -4\pi R^2 en_\infty \exp\left(\frac{-e|\phi_D|}{k_B T_e}\right) \sqrt{\frac{k_B T_e}{2\pi m_e}}. \quad (2.32)$$

In case of a positively charged particle, the role of the ions and electrons is reversed, in the sense that in that case the ion current has the Boltzmann factor, and the electron current the linear term, with opposite sign.

In equilibrium, the electron and ion current to the dust particle will be equal. This means that the dust particle surface potential can be found from

$$-\exp\left(\frac{e\phi_D}{k_B T_e}\right) \sqrt{\frac{k_B T_e}{2\pi m_e}} + \sqrt{\frac{E_s}{2m_+}} \left(1 - \frac{e\phi_D}{E_s}\right) = 0. \quad (2.33)$$

Defining the effective dust particle potential $\Psi_D = -e\phi_D/k_B T_e$ and $z = k_B T_e/E_s$, $\alpha = m_+/m_e$, we can rewrite the above as

$$^2 f(\mathbf{v})d^3v = n_+ \left(\frac{m_+}{2\pi k_B T_+}\right)^{3/2} \exp\left(\frac{-m_+ \mathbf{v}^2}{2k_B T_+}\right) d^3v$$

$$\exp(\Psi_D) - \sqrt{\frac{\pi}{z\alpha}}(1 - z\Psi_D) = 0, \quad (2.34)$$

which can be solved numerically for different values of z and m_+ . For argon ions at room temperature, probe theory gives an approximate value for the effective floating potential with respect to the plasma potential of $\Psi_D = \Psi_f \approx -5$ [8].

The charge carried by the dust particle $Q_D = 4\pi R^2\sigma$, with σ the surface charge density, which is given by $\sigma = -\epsilon_0\nabla(V)_{r=R}$, is then found by filling in the screened Coulomb potential of equation 2.17, which gives

$$Q_D = 4\pi\epsilon_0 R \left(1 + \frac{R}{\lambda_D}\right) \Psi_D \frac{k_B T_e}{e}. \quad (2.35)$$

Usually, the linearized Debye length is much larger than the particle radius (which is a requirement for the validity of the derived OML currents). Thus, the above becomes for a dust particle in argon plasma,

$$Q_D = 4\pi\epsilon_0 R \Psi_D \frac{k_B T_e}{e} \approx -\frac{20\pi\epsilon_0 k_B T_e}{e} R. \quad (2.36)$$

Therefore, at given electron temperature, the dust charge is a linear function of the particle radius only.

Ion-neutral collisions

The above OML derivation of the dust charge does not include ion-neutral collisions, in which energy and angular momentum might be lost by the ion, i.e. charge-exchange collisions. Suppose now that an ion, which originally has too much angular momentum to be captured, collides with a neutral atom and loses angular momentum. It is then possible that the ion *does* enter the solid angle for capture by the dust particle. This means that charge-exchange collisions can increase the ion collection current. This is true as long as the ions can not gain energy and angular momentum in collisions with neutrals. We assume here that the ions thermalize rapidly in these collisions, so that they are in thermal equilibrium with the neutrals, ruling out hot neutral populations.

In [9], an approximation was derived for the extra ion flux due to these collisions. It was stated that any ion having a charge-exchange collision closer to the particle than the radius for which its thermal energy equals the potential at that radius, dubbed r_T , will eventually be captured by the dust particle. For small β (equation 2.24), r_T exactly equals the Coulomb-radius, ρ_0 , whereas for intermediate values, $\beta \sim 1$, it is equal to λ_D . The probability that such a collision will happen scales approximately as the ratio of r_T over the average mean-free path of

the ions, l_{mfp} . The extra flux of ions to the dust particle due to the collisions is then given by,

$$F_{coll} = \left(\frac{r_T}{R}\right)^2 \frac{r_T}{l_{mfp}} F_{th}, \quad (2.37)$$

where F_{th} is the thermal flux of ions in the ambient plasma. In [10] an expression was derived for the total ion current for $0.1 \lesssim \beta \lesssim 10$, (which are values important for the discharges modelled, as shown both in our simulations in chapter 5 as well as in experiments [11]) which is written as

$$I_{+,tot} = -4\pi R^2 e n_+ \sqrt{\frac{E_s}{2m_+}} z \Psi_D \left(1 - 0.1 z \Psi_D \frac{\lambda_D}{l_{mfp}}\right). \quad (2.38)$$

It is important that even though λ_D/l_{mfp} might not be very large, $z\Psi_D$ can be, so that the charge-exchange collisions are still important for the dust particle charging.

Electron depletion and the Havnes parameter

Another important effect not yet considered is strong electron depletion by the dust. When the dust density is high, many electrons are lost from the plasma volume. This can lead to a situation where the dust charge becomes much less negative than predicted by the OML currents. We can show this by starting at equation 2.33, but in stead of assuming simple quasi-neutrality, we use the complete form of the quasi neutrality equation, $n_e - n_+ + Z_D n_D = 0$ to substitute for n_+ . Defining the *Havnes parameter* [12], $P = n_D Z_D / n_e$, this leads to,

$$\exp(\Psi_D) - \sqrt{\frac{\pi}{z\alpha}} (1 + P) (1 - z\Psi_D) = 0. \quad (2.39)$$

We see that for increasing P , which means for increasing depletion of free electrons from the plasma, the positive contribution to the charging becomes larger, leading to a reduction of the number of electrons carried by the dust. Figure 2.6 also shows this. In chapter 7 this also plays a role.

Charging time

When a dust particle is introduced to the plasma, the electrons will be able to reach the dust particle first, due to their high mobility. After some time, the dust particle becomes negatively charged, repels electrons and attract ions. This means that the final dust equilibrium is determined by the *ions* and not the electrons. An estimate for the final charging time can then be found from

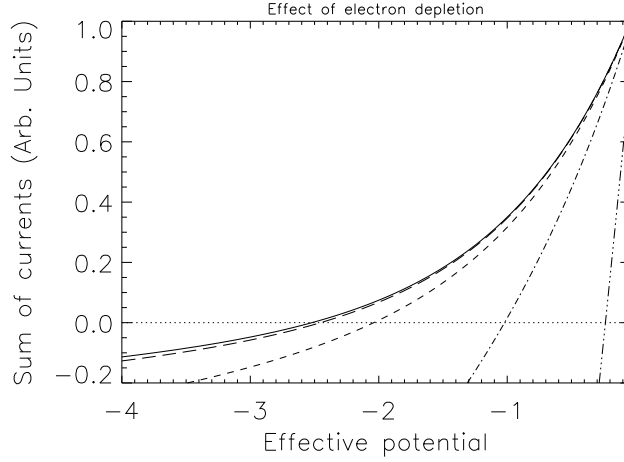


Figure 2.6: The sum of the currents of equation 2.39, for argon with $z = 120$. When it equals 0, the effective dust particle potential, Ψ_D , equals the floating potential. The different lines correspond to, solid line: $P = 0$ (no electron depletion), dashed line: $P = 0.1$, short dashed line: $P = 1$ (just above typical electron depletion), dot-dash line: $P = 10$ (very high electron depletion), dot-dot-dot-dash line: $P = 100$. We see that the dust charge without depletion (solid black line) is closer to $\Psi_D \sim -3$ (-2.6) than $\Psi_D \sim -5$.

$$\frac{dQ_D}{dt} = 4\pi R^2 n_+ e \sqrt{\frac{E_s}{2m_+}} \left(1 - \frac{e\phi_D}{E_s} \right), \quad (2.40)$$

Inserting a solution of the form $Q_D(t) = C_1 \exp(-t/\tau_{ch}) + C_2$, representing a charging curve of a capacitor, with τ_{ch} the "RC-time", which is the time needed to charge a capacitor through a resistor in a RC-circuit, we find,

$$-\frac{1}{\tau_{ch}} C_1 \exp\left(\frac{-t}{\tau_{ch}}\right) = 4\pi R^2 n_+ e \sqrt{\frac{E_s}{2m_+}} \left(1 - \frac{e(C_1 \exp(\frac{-t}{\tau_{ch}}) + C_2)}{4\pi\epsilon_0 R E_s} \right). \quad (2.41)$$

For the limit $t \rightarrow \infty$, we must have $C_2 = 4\pi\epsilon_0 R E_s / e$. Filling this in, results in the solution for the charging time τ_{ch} ;

$$\tau_{ch} = \frac{\epsilon_0 E_s}{e^2 R n_+ \sqrt{\frac{E_s}{2m_+}}}. \quad (2.42)$$

For an one micron radius dust particle in an argon plasma at room temperature with negligible ion drift and typical densities of $n_+ \sim 10^{15} \text{ m}^{-3}$, charging times

are in the order of $10^{-6} \text{ s} < \tau_{ch} < 10^{-5} \text{ s}$. This means that for our simulations $\tau_{RF} = 1/\nu_{RF} < \tau_{ch} < \tau_D$, with τ_D a typical dust time scale, which can be the inverse dust plasma frequency, $\tau_D = 2\pi/\omega_{p,D} = 2\pi(\sqrt{n_D Q_D^2/m_D \epsilon_0})^{-1}$. In the quasi-neutral bulk, the dust charge can be assumed to be constant during a RF-cycle, whereas for the movement of the dust, we can assume it is adjusted instantaneously. In the sheaths however, during part of the RF-cycle, the electrons are swept away by the time varying electric field. This means that ions temporarily are able to reduce the negative charge. This is further shown in [13].

Charging mechanisms

Up to now, only charging by collection of plasma has been considered. Of course, different mechanisms of (de-)charging are possible. We will discuss the different charging mechanisms in dusty plasma and show whether or not they are of importance for this thesis. An extended discussion of the different charging mechanisms in (astrophysical) dusty plasma can be found in [14]. The different charging mechanisms include:

- **Field emission.** Charged particles can be emitted from a surface when the local electric field is high enough. Assume we have a spherical particle with radius R and a surface charge density σ (C m^{-2}). The electric field at the surface is then given by $E = \sigma/\epsilon_0$, and the electrostatic pressure on the surface charges is given by $P = \epsilon_0 E^2/2$, which acts outwards, against the forces binding the charges onto the surface.

Suppose we now want to lift this charged surface away from the particle. The work required to do so is $\Delta U = P \cdot \Delta V$, with ΔV the change in volume. This is roughly given by $4\pi R^2 \cdot \Delta r$. Typical binding energies of band electrons in metals, or electrons on carbon nanotubes is in the range of (1-6) eV. If we then lift the charged surface over roughly an inter-atomic distance ($\Delta r \sim 10^{-10} \text{ m}$), and require that the work done by the electrostatic pressure has to exceed typical binding energies, we can solve for the required electric field; $P \cdot 4\pi R^2 \Delta r > (1 - 6) \text{ eV}$; $\epsilon_0 E^2 2\pi R^2 \Delta r > (1 - 6) \text{ eV}$; $E > 5.4\sqrt{(1 - 6)} R^{-1} \text{ V m}^{-1}$. For a $1 \mu\text{m}$ particle, we then find a required electric field at the surface of $E \approx 9 \text{ V } \mu\text{m}^{-1}$. Surprisingly, this corresponds to only 6500 electron charges.

Of course, no quantum mechanical effects were taken into account, and the above derivation underestimates the observed electric fields. In multiwall carbon nanotube field emitters used in novel field emission displays, the electric field at the surface is roughly $20 \text{ V } \mu\text{m}^{-1}$ [15]. For metal tip field emitters, such as used in field emission microscopes, it can be as large as $1\text{-}10 \text{ V nm}^{-1}$ [16].

Such strong fields then require sharp points or edges, which locally enhance the macroscopic field. However, in this thesis we only present results of particles which are assumed to be perfectly spherical, so that field emission plays no role. In many experiments, specially fabricated dust particles are used, which are spherical, or have other pre-defined shapes, but are typically very smooth. In-situ grown particles can have a different shape, for instance fractal-like. In that case, field emission might play an important role, also for smaller particles. It results in a reduction of the number of electrons carried by the dust.

- **Photo-detachment.** When photons with energies above the work function interact with the dust, electrons can be removed through the effect of photo-detachment. Many plasmas in space are exposed to intense ultraviolet radiation, for instance plasmas around young stars, as discussed in chapter 1 and also the dusty plasma in the ionosphere. In fusion reactors there can also be significant UV fluxes [17]. Plasma itself can also emit UV radiation, even though the intensity is relatively weak, however, commercially available UV sources are abundant, which could provide an interesting tool to control dust charge in laboratory dusty plasmas. This is investigated in chapter 7.
- **Radio-active emission.** When dust particles consist of radio-active material, electrons (via β -decay) or α particles can be emitted. Depending on the material, this can result in either more positive dust, or more negative dust. In this thesis we do not consider radio-active dust, but in fusion plasmas, carbon dust can absorb tritium from the plasma, which is radio-active and decays emitting an electron. In space, radio-activity might also play an important role.
- **Thermionic emission.** When dust particles are heated, for instance by recombination of the collected charged plasma particles, the electrons and ions collected on the surface gain thermal energy. When this energy becomes larger than the binding energy, the collected particles can be emitted into the plasma [18, 19]. For negatively charged particles this is most likely for the electrons, due to the repelling potential. In [20] it was shown that the particle heating in typical experiments modelled in this thesis is very small. Therefore, we do not include it here.
- **Tribo-electric emission.** When two particles come in contact, surface friction can transport electrons from one to the other. In this thesis, dust particles carry a significant amount of charge. Due the repulsive force between

them, they are always well separated. Nanometer sized particles carry only few charges, which means they are more likely to come in contact.

- **Secondary electron emission by electrons or ions.** When electrons and ions are accelerated to large energies, they might release electrons from the surface when they collide with the dust. For secondary electron emission to become effective, high impact energies are required ($\gtrsim 50eV$), which are not present in large quantities, as calculations in chapter 7 will show. Therefore, we do not include this effect here.

2.3 Forces acting on dust particles

Charged particles in plasma experience several forces and settle in equilibrium positions according to the way these forces act. The first and most obvious force is that of gravity. Dust particles in the micrometer range are in general massive enough to experience a significant gravitational force.

Since electric fields are present in plasma, charged objects are accelerated in these fields. Furthermore, they capture and deflect charged plasma particles. Especially ions are heavy enough to transfer a significant amount of momentum to the dust, which results in the so called ion drag force. This force depends on the dust charge, but also on charge-exchange collisions, the non-linearity of the screening of the dust by the plasma, and on the ion flow speed.

Due to the low ionization degree, dust-neutral collisions are abundant. This means that dust particles moving through a discharge experience a neutral drag force. Since the neutral atoms can be heated by collisions with ions, there is a difference in the amount of momentum transferred to the dust on the side of the dust particle facing a hotter neutral gas volume, than on the side facing a colder volume. This results in a net force called the thermophoretic force.

Finally, the screened charged particles interact with each other through the screened Coulomb potential, once they get close enough to each other. This interaction is an important source of internal pressure and plays a role in the diffusion of charged dust.

We will give the mathematical forms of these forces and illustrate their importance by calculating their magnitudes for dust particles with a radius of 2 micrometer and a mass density of 2000 kg m^{-3} in typical plasma parameters.

2.3.1 Electrostatic force

The highly charged dust particles interact with electric fields due to space charges, or due to externally applied electric fields. They will be accelerated in the time-

averaged electric field $\bar{\mathbf{E}}$, and the corresponding force is given by [21]

$$\mathbf{F}_{\bar{E}} = Q_D \bar{\mathbf{E}} \left(1 + \frac{(R/\lambda_D)^2}{3(1 + (R/\lambda_D))} \right). \quad (2.43)$$

The term between brackets is due to the polarization of the dust charge by the plasma around the dust particle, which causes a dipole term to arise. (Higher order terms are neglected.) For $R \ll \lambda_D$, the usual form for the electrostatic acceleration is found, which is used from here on,

$$\mathbf{F}_{\bar{E}} = Q_D \bar{\mathbf{E}}. \quad (2.44)$$

Since $Q_D \propto R$, we see that this force scales linearly with R . For a particle with a 2 micrometer radius, the typical charge in the quasi-neutral bulk of the discharges modelled in this thesis is approximately $Z_D \leq 10^4 e$, whereas the electric field in the bulk is approximately $\bar{E} \sim 10^2 \text{ V m}^{-1}$. This gives an electrostatic force of $F_{\bar{E}} \sim 1.6 \cdot 10^{-13} \text{ N}$. In the sheath region in front of the electrodes the dust charge is smaller, $Z_D \sim 10^3 e$, but the electric field is much higher, $\bar{E} \sim 10^4 \text{ V m}^{-1}$. This gives a force of $F_{\bar{E}} \sim 1.6 \cdot 10^{-12} \text{ N}$.

2.3.2 Gravity

On Earth, particles are accelerated by the force of gravity, which has an average value of $\mathbf{g} = -g \hat{\mathbf{z}} = -9,81 \text{ m s}^{-2} \hat{\mathbf{z}}$. For a dust particle with mass density ρ , this force is given by

$$\mathbf{F}_g = \frac{4\pi\rho R^3}{3} \mathbf{g}. \quad (2.45)$$

This force scales with the volume of the particle, $F_g \propto R^3$. For nanometer sized particles in typical laboratory discharges it is therefore an unimportant force, while for micrometer sized particles it is an important force, playing a dominant role in the spatial ordering and equilibrium positions of the particles in the plasma.

For our test particle we find a gravitational force of $F_g = 6.6 \cdot 10^{-13} \text{ N}$. We see that the force of gravity can not be balanced by the electric field in the bulk of the discharge, but only in the sheath regions in front of the electrodes. In order to study the full three dimensional structure and dynamics of dusty plasma of micrometer sized particles, micro-gravity experiments are required.

2.3.3 Ion drag force

The ion drag comes from the interaction between ions and charged dust particles. Ions are both collected and scattered, and transfer momentum to the dust. In

general form it can be described as [22],

$$\mathbf{F}_{ion} = m_+ \int \mathbf{v} v f_+(\mathbf{v}) [\sigma_c(v) + \sigma_s(v)] d\mathbf{v}. \quad (2.46)$$

with \mathbf{v} the ion velocity, $v = |\mathbf{v}|$, $f_+(\mathbf{v})$ the ion velocity distribution function, $\sigma_c(v)$ and $\sigma_s(v)$ the ion collection momentum transfer and ion scattering momentum transfer cross-section. The collection cross section was already derived in the section on dust particle charging, so that we simply have from equation 2.27, $\sigma_c = \pi b_c^2 = \pi R^2(1 - e\phi_D/E_s)$.

The derivation of the scattering cross section is as yet an unsolved problem for all possible values of the ion flow speed. Furthermore, the non-linear screening of dust particles in plasma is important for ion-dust interaction, as well as the presence of ion-neutral collisions, similar to the problem of dust charging. The original approach [5] assumes only linear scattering of ions very close to the dust particle, which is called *small angle scattering*³.

Small angle scattering

The general form of the scattering cross section for ions approaching very close to the dust particle, so that they move through the unscreened Coulomb potential, is given by [22],

$$\sigma_s(v) = 4\pi \int_{\rho_{min}}^{\rho_{max}} \frac{\rho d\rho}{1 + (\rho/\rho_0(v))^2}, \quad (2.47)$$

where the integration is over all the scattering impact parameters ρ between the minimum impact parameter for capture, $\rho_{min} = b_c$, as given above, and the maximum scattering impact parameter ρ_{max} , which is yet to be determined. $\rho_0(v)$ is the Coulomb radius for arbitrary ion velocity v , so that $\lim_{v \downarrow v_T} \rho_0(v)$ is ρ_0 as defined in equation 2.19. The solution to the above equation is given by $\sigma_s(v) = 4\pi\rho_0^2(v)\Lambda(v)$, with $\Lambda(v)$ the Coulomb logarithm,

$$\Lambda(v) = \ln \left[\frac{\rho_0^2(v) + \rho_{max}^2(v)}{\rho_0^2(v) + b_c^2(v)} \right]^{1/2}. \quad (2.48)$$

In the small angle solution, it is then assumed that the maximum scattering impact parameter is given by the Debye length, $\rho_{max} = \lambda_D$, so that the scattering cross-section becomes,

³In a way this is an interesting name, since usually *small angle scattering* refers to scattering of projectiles in orbits far away from the scattering target, over tiny deflection angles, like in X-ray scattering. Here it means that ion scattering takes place well outside the radius where $eV_D/k_B T_+ > 1$, but not necessarily over "small angles".

$$\sigma_s(v) = 4\pi\rho_0^2(v) \ln \left[\frac{\rho_0^2(v) + \lambda_D^2}{\rho_0^2(v) + b_c^2(v)} \right]^{1/2}. \quad (2.49)$$

This can be rewritten, using $\beta(v) = \rho_0(v)/\lambda_D$, to

$$\sigma_s(v) = 2\pi\rho_0^2(v) \ln \left[\frac{1 + \beta^2(v)}{\beta^2(v) + b_c^2(v)/\lambda_D^2} \right]. \quad (2.50)$$

This form implies that the ions scattered with impact parameters larger than the Debye length do not transfer a significant amount of momentum to the dust, which is only true for very small values of $\beta(v)$. This is typically not so for dust grains in a plasma, as was shown in section 2.2.3. Therefore, the effect of scattering over large angles needs to be taken into account.

Large angle scattering

Taking interactions beyond the Debye length into account, one needs to redefine the maximum impact parameter ρ_{max} . The cut-off condition in terms of the distance of closest approach for an ion, r_0 , becomes $r_0(\rho_{max}(v)) = \lambda_D$. By analogy, in [13], the maximum impact parameter corresponds to an ion grazing an imaginary sphere with radius λ_D . Similar to the OML collection radius, we then find $\rho_{max}(v)$ as,

$$\rho_{max}(v) = \lambda_D \sqrt{1 - \frac{e\phi(r = \lambda_D)}{E_s}} = \lambda_D \sqrt{1 + 2\beta(v)}. \quad (2.51)$$

Any ion approaching the dust with energy $E_s = mv_+^2/2$ with an impact parameter less than or equal to $\rho_{max}(v)$ then contributes to the scattering momentum transfer. Using this in equation 2.48, we have

$$\Lambda(v) = \frac{1}{2} \ln \left[\frac{\rho_0^2(v) + \lambda_D^2 + 2\lambda_D\rho_0(v)}{\rho_0^2(v) + R^2 + 2R\rho_0(v)} \right] = \ln \left[\frac{1 + \beta(v)}{\beta(v) + R/\lambda_D} \right]. \quad (2.52)$$

This then is used to calculate the scattering cross-section taking non-linear scattering of ions beyond the Debye length into account, but still by assuming an unscreened Coulomb potential. The above form is valid for $\beta(v) \lesssim 5$, and therefore only covers moderate non-linearity. For the case of collection and moderate non-linear scattering of ions, we thus find an ion drag equal to,

$$\mathbf{F}_{ion} = m_+\pi R^2 \int \mathbf{v} v f_+(\mathbf{v}) \left[\left(1 + 2\frac{\rho_0}{R}\right) + \frac{4\rho_0^2}{R^2} \ln \left(\frac{1 + \beta}{\beta + R/\lambda_D} \right) \right] d\mathbf{v} \quad (2.53)$$

where ρ_0 , λ_D , and β depend on v .

A typical form used for the ion distribution function, $f_+(\mathbf{v})$, is a so called shifted Maxwellian distribution. After integrating the above with this distribution, a simple analytical form of the scattering ion drag force is obtained in the limit $u_+ < v_T$. To allow for a larger range of drift velocities, the mean velocity, v_+ is used, as defined in section 2.2.3. The differences in the results with the complete solution to the integral [23] are small for the discharges under consideration, as is also mentioned in chapter 3. Since our approach is computationally more robust and straightforward, we use the analytical form. This way, we find for the ion drag force,

$$\mathbf{F}_{ion} = n_+ m_+ v \mathbf{u}_+ \left[\pi R^2 \left(1 + \frac{2\rho_0}{R} \right) + 4\pi\rho_0^2 \ln \left(\frac{1 + \beta(v)}{\beta(v) + R/\lambda_D} \right) \right], \quad (2.54)$$

for moderate non-linear scattering. Depending on the mean free path, as well as on the particle potential, ion-neutral collisions can play an important role in the momentum transfer, similar to the way these collisions change the dust charging.

Ion-Neutral collisions

In [24, 25], the appropriate form of the collision operator was derived for sub-thermal ion flow, with $x = \lambda_D/l_{mfp}$ as,

$$\mathcal{K}(x) = x \arctan(x) + (\sqrt{\pi/2} - 1)(x^2/(1+x^2)) - \sqrt{\pi/2} \ln(1+x^2),$$

so that the ion drag including ion-neutral collisions, and moderate non-linearity, is given by

$$\mathbf{F}_{ion} = n_+ m_+ v \mathbf{u}_+ \times \left(\pi R^2 \left(1 + \frac{2\rho_0}{R} \right) + \pi\rho_0^2 \left[4 \ln \left(\frac{1 + \beta(v)}{\beta(v) + R/\lambda_D} \right) + \mathcal{K} \left(\frac{\lambda_D}{l_{mfp}} \right) \right] \right). \quad (2.55)$$

Ion flow

In order to take the screening anisotropy caused by ion flow into account, an analytical approach has been derived in a recent Particle-In-Cell approach [26]. The mean ion energy as used in the calculation of the Coulomb logarithm, has to be changed according to,

$$\begin{aligned}
\frac{1}{2}m_+v_+^2 &= \frac{4k_B T_+}{\pi} + \frac{1}{2}m_+u_+^2 \\
&\quad \updownarrow \\
\frac{1}{2}m_+\tilde{v}_+^2 &= \frac{4k_B T_+}{\pi} + \frac{1}{2}m_+u_+^2 \left[1 + \left(\frac{u_+}{u_B} / (0.5 + 0.05 \ln \left(\frac{m_+}{Z_+} \right) + \sqrt{\frac{T_+}{T_e}}) \right)^3 \right].
\end{aligned} \tag{2.56}$$

$u_B = \sqrt{k_B T_e / m_+}$ is the Bohm velocity, and $m_+ / Z_+ = 40$ for argon. It was shown [26], that this form becomes significant when $u_+ \geq 0.55u_B$. This way, the final form of the ion drag, including ion-neutral collisions, moderate non-linearity, and significant ion flow becomes,

$$\begin{aligned}
\mathbf{F}_{ion} &= n_+ m_+ v \mathbf{u}_+ \times \\
&\quad \left(\pi R^2 \left(1 + \frac{2\rho_0}{R} \right) + \pi \rho_0^2 \left[4 \ln \left(\frac{1 + \beta(\tilde{v})}{\beta(\tilde{v}) + R / \lambda_D(\tilde{v})} \right) + \mathcal{K} \left(\frac{\lambda_D}{l_{mfp}} \right) \right] \right).
\end{aligned} \tag{2.57}$$

For supersonic ion flow, $\beta(\tilde{v}) \downarrow 0$, so that the small angle scattering approach is valid, but with the electron Debye length as the screening length, which follows automatically from the definition of the linearized Debye length, for $M_T \gg 1$.

According to [23] the effect of finite grain size is important when $\beta(v) \lesssim R / \lambda_D \ll 1$, which happens when $M_T \gtrsim \sqrt{z\chi}$. Here $\chi = e |\Psi_D|$, the dimensionless grain charge, and $z = T_e / T_i$. Since $z\chi \gtrsim 100$, we have the effect of finite grain size for $M_T \gtrsim 10$, in which case the Coulomb logarithm becomes $\Lambda \approx \ln(\lambda_D / R)$. The collection force becomes more important than the scattering force for large ion flow in the sheaths. This happens when $M_T \gtrsim \sqrt{z\chi} / 8 \ln(\lambda_e / R)$, which is about $M_T \gtrsim 20$. In typical discharges modelled here, most of the bulk of the discharges is sub-thermal and shows moderate non-linearity. Near the sheaths, the ion flow quickly rises up to the point where collection dominates. Therefore, the above form used for the ion drag force is suitable for our calculations.

Taking ions streaming with $M_T = 1$, temperature $T_+ = 293K$, and assuming that the density of interacting ions is the same as the ions in the unperturbed plasma $n_+ \approx n_{+, \infty}$, the magnitude of the ion drag force for $\beta \sim 5$ is $F_{ion} \sim 800\sqrt{2} \ln(1.2) m_+ v_T^2 \epsilon_0 k_B T_+ / e^2 \sim 1.7 \cdot 10^{-12}$ N. We see that $F_{ion} \approx F_{\bar{E}}$.

2.3.4 Neutral drag force

The ionization fraction in typical experiments is very low. Therefore, the most important constituent of the plasmas in such experiments will simply be the neutral gas. Dust particles moving through the background gas will experience many

collisions with neutral particles, resulting in a friction force. This friction force is called the neutral drag force. The original derivation of the force acting on spheres moving through a flowing background is given in [27].

For a dust particle velocity relative to the background, \mathbf{V} , spherical particles with radius R , moving through the background of density n_n , mass m_n , with an average velocity $v_T = \sqrt{8k_B T_{gas}/\pi m_n}$, the neutral drag force is given by:

$$\mathbf{F}_{nd} = -\frac{4}{3}\pi R^2 n_n m_n v_T \mathbf{V}. \quad (2.58)$$

This equation is correct for specular reflection of neutral particles colliding with the dust. This force is proportional to the square of R .

For argon plasma ($m_{ar} = 40 m_p$) at room temperature $T = 293K$, at typical pressures between 100 and 300 mTorr (13 and 40 Pa), we find a neutral drag force $1.42 \cdot 10^{-12} V \leq F_{nd} \leq 4.35 \cdot 10^{-12} V$ N. Typical relative dust flow speeds will turn out to be in the range of cm s^{-1} , or even mm s^{-1} . This gives a neutral drag force in the range of $F_{nd} \sim 10^{-15} - 10^{-14}$ N. This force is small compared to gravity and the electrostatic force. It plays an important role in the time needed for dust to reach equilibrium positions when introduced into the plasma, but also damps waves moving through a dust cloud, or oscillations of dust particles. For a completely dynamic calculation of the dust transport one would therefore have to include the $\partial_t + \mathbf{v} \cdot \nabla \mathbf{v}$ term in the dust transport, but this is beyond the aim of this thesis, where the calculations are based on the equilibrium solution.

2.3.5 Thermophoretic force

Ions collide with neutral atoms and locally heat the neutral background gas. This leads to temperature gradients. A further source of gas heating could be heating by the walls. When neutral atoms are scattered off the walls, which are at a higher temperature, they could come off the wall with a higher temperature themselves. Ions and electrons recombining, can also result in hot neutral atoms [28].

These neutral atoms impinge on dust particles, during which they transfer momentum to the dust. More neutral atoms will hit the side facing the hot part of the gas per second, than on the side facing the colder part of the background gas. Furthermore, hotter atoms will on average transfer more momentum per collision than cold atoms. Therefore, the dust particles will experience a net force against the temperature gradient. This force is called thermophoresis, and can be calculated as,

$$\mathbf{F}_{th} = -\frac{32 R^2}{15 v_T} \kappa_T \nabla T_n, \quad (2.59)$$

where κ_T is the thermal conductivity coefficient for Argon gas, which at 300 K has a value of $0.01772 \text{ W K}^{-1} \text{ m}^{-1}$. This force is again proportional to the square of R .

In [20] it was found that typical temperature gradients in the PKE (Plasma Kristall Experiment) chamber are in the range of 100 K m^{-1} . This results in a thermophoretic force of $F_{th} \sim 9.6 \cdot 10^{-15} \text{ N}$. Like the neutral drag force, thermophoresis plays only a minor role for micrometer sized dust particles in the discharges modelled in this thesis. Sometimes heated electrodes are used to create a temperature gradient in discharges, large enough to balance the force of gravity. This allows the study of three-dimensional dust structures, without the need for micro-gravity environments [29], but requires large experimental efforts to reduce inhomogeneities in the temperature profile.

2.3.6 Mutual Coulomb interaction

One can imagine that a dust cloud consisting of highly charged particles at large densities is much harder to compress or deform than a cloud consisting of particles with a low charge at low densities. A measure for this is given by the *coupling parameter*, $\Gamma = E_{Coul}/E_{th} = (Q_D^2 \exp(-\Delta/\lambda_D)/4\pi\epsilon_0\Delta)/(k_B T_D)$, where we have defined the thermal energy as $E_{th} = k_B T_D$ and $\Delta \approx n_D^{-1/3}$ is the average inter-particle distance.

When $\Gamma \gg 1$, the coupling between the dust particles is very strong and the dust forms an incompressible crystal. The dust pressure for such a crystal was derived in [30] as,

$$P_{c,D} = \frac{1 + \alpha\kappa}{3} N_{nn} \tilde{\Gamma} P_{D,g}, \quad (2.60)$$

with α a geometrical factor, which depends on the type of crystal ordering of the particles. $\alpha = 1.12$ for face centered cubic (fcc) and hexagonal closed packing (hcp) crystals, which both have a number of nearest neighbors, $N_{nn} = 12$. $\tilde{\Gamma}$ is then a "geometrically corrected" coupling parameter, with $\Delta \rightarrow \alpha\Delta$. $P_{D,g} = n_D k_B T_D$ is the simple dust "gas-phase" pressure for $\Gamma \ll 1$, and $\kappa = \Delta/\lambda_D$.

In between $\Gamma \ll 1$ and $\Gamma \gg 1$, we are not aware of any analytical solutions. In [30] a linear interpolation is used, such that $P_D = P_{D,g}(1 - x) + P_{D,c} x$, where $x = (\Gamma - 1)/(\Gamma_c - 1)$, and $\Gamma_c = 106 \exp \kappa / (1 + \kappa + \kappa^2/2)$ is the value of Γ beyond which the dust is assumed to be in a crystalline state.

Using the above pressure equation, we can define the dust diffusion coefficient as,

$$D_D = \frac{dP_D}{dn} \frac{1}{m_D \nu_{m,D}}, \quad (2.61)$$

with $\nu_{m,D} = 4\pi R^2 n_n v_T (m_n/m_D)/3$ the dust-neutral momentum transfer frequency, which has a value in the order of 10^2 s^{-1} , and $v_T = \sqrt{8k_B T_n/\pi m_n}$ the neutral atom thermal velocity [11]. The role of this diffusion is to smoothen out the dust density and act against the compressing action of the ion drag and electrostatic force.

2.3.7 Summary

We have seen that for the transport of micrometer sized particles, the electrostatic force, gravity, and the ion drag are the dominant forces. Thermophoresis is not important for most discharges modelled in this thesis. For smaller particles thermophoresis can be important. Neutral drag mainly determines the time-scale on which an equilibrium position is reached and damps small scale dust dynamics. Finally, the mutual Coulomb interaction sets the diffusion of the dust particles.

2.3.8 Void formation

In experiments in sounding rockets, or on board of the International Space Station [31], gravity no longer plays its dominant role. Therefore, ion drag and the electrostatic force are the most dominant forces. Ionization in the center of the discharge results in ions diffusing outwards in the time averaged electric field, which form a dust free void region. Figure 2.7 shows the difference between a ground-based experiment and an experiment under micro-gravity conditions.

The Coulomb interaction between the charged particles determines the thickness of dust layers, but also the compressibility and diffusion of dust clouds. For the appearance of a dust cloud in the final equilibrium, the ion drag, electrostatic force, and the mutual Coulomb interaction are then the most important forces.

2.4 Simulation models

Except for the results presented in chapter 4, the chapters of this thesis are based on different simulation models. This section describes what our models solve and how they do so. First, we will describe a *fluid model*, which solves time-averaged quantities in two dimensions. Second, we explain how our *Particle-In-Cell model* follows many particles in a one-dimensional dusty argon plasma.

2.4.1 Fluid model

The fluid model [32, 33, 34] solves the particle balance for both the electrons and the ions in two dimensions in a cylindrical geometry. The particle balance for

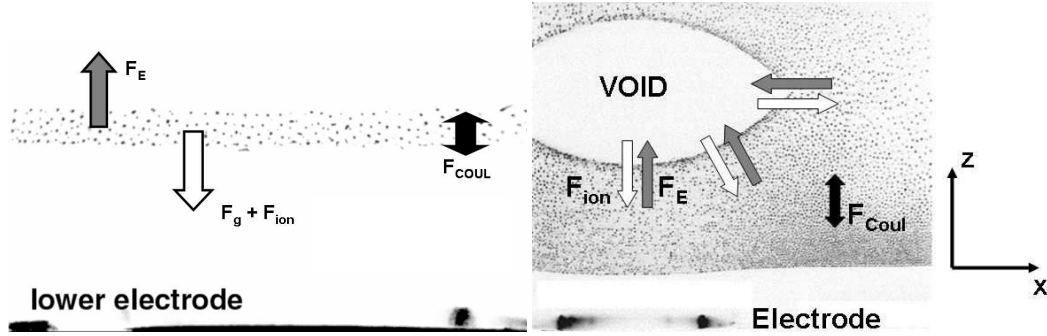


Figure 2.7: **Left:** Side view of a typical dusty plasma experiment in a ground-based laboratory. Gravity dominates and only allows a thin two-dimensional layer in which the sheath electric field acts as the balancing force. The mutual repulsion determines the thickness of the layer.

Right: Without the force of gravity a three-dimensional dust crystal forms. Due to the plasma production in the center, ions diffuse outwards and cause a strong radial ion-drag force, which acts against the electrostatic force. This results in a dust-free void region. The mutual Coulomb repulsion determines the compressibility of the crystal.

species j is written as,

$$\frac{\partial n_j}{\partial t} = -\nabla \cdot \Gamma_j + S_j, \quad (2.62)$$

which is a mathematical translation of the statement that the change in time of the particle density n_j equals the net flux Γ_j of the particles over the boundary of the volume, plus the creation and destruction of the quantity inside the volume, with source terms S_j . As was explained before, only collisions between charged plasma particles and neutrals are considered, due to the low ionization degree.

Assuming a distribution function which is isotropic in the direction perpendicular to the flux [32], the particle flux can be expressed using the so called *drift-diffusion approximation*,

$$\Gamma_j = \mu_j n_j \mathbf{E} - D_j \nabla n_j, \quad (2.63)$$

with μ_j , and D_j the mobility and diffusion coefficients respectively. The electric field is found by solving the Poisson equation, including the dust charge calculated at every grid point using the OML currents, equation 2.31, 2.32, with the calculated plasma quantities as input;

$$\nabla^2 V = \frac{e}{\epsilon_0} (n_e - n_+ + n_D Z_D), \quad (2.64)$$

$$\mathbf{E} = -\nabla V.$$

For the electrons this instantaneous field is used, however, the ions are too heavy to follow the RF field, therefore, an effective field $\mathbf{E}_{eff,+}$ is calculated using the ion-neutral momentum transfer frequency, $\nu_{m,+} = e/\mu_+m_+$,

$$\frac{d\mathbf{E}_{eff,+}}{dt} = \nu_{m,+} (\mathbf{E} - \mathbf{E}_{eff,+}). \quad (2.65)$$

The energy balance is also solved, however, only for the electrons. The ions are assumed to deposit their thermal energy locally in charge-exchange collisions [35]. For the electron energy density w_e , a similar drift-diffusion approximation is used to solve the second moment of the Boltzmann equation,

$$\begin{aligned} \frac{\partial w_e}{\partial t} &= -\nabla \cdot \Gamma_{w_e} + \mathbf{J}_e \cdot \mathbf{E} + S_{w_e}, \\ \Gamma_{w_e} &= -\frac{5}{3}\mu_e w_e \mathbf{E} - \frac{5}{3}D_e \nabla w_e, \end{aligned} \quad (2.66)$$

where the term $\mathbf{J}_e \cdot \mathbf{E}$ is Ohmic heating of the electrons in the electric field. The source terms for energy and particles include electron-impact excitation, ionization, charge-exchange, but of course also recombination of plasma on the dust particles. So both for the electric field, as well as for the source-terms, are the plasma equations coupled to the dust equations.

For the transport of the dust, the electrostatic, ion drag, and thermophoretic force are assumed to be in balance with the neutral drag at every time step of the simulation. This way, we can solve for the dust flux, using a drift-diffusion type of equation,

$$\Gamma_D = \frac{n_D \mathbf{F}_{\bar{E}}}{m_D \nu_{m,D}} - D_D \nabla n_D + \frac{n_D \mathbf{F}_{th}}{m_D \nu_{m,D}} + \frac{n_D \mathbf{F}_{ion}}{m_D \nu_{m,D}}. \quad (2.67)$$

These equations form a closed set. Initially, no dust is introduced and the code is run until a periodic solution for the plasma quantities is found, so that the set of solutions, $U(t)$, obeys $U(t) = U(t + \tau_{RF})$. When this is achieved (the code is said to "converge"), source terms for the dust are added, corresponding to approximately $7.5 \cdot 10^5$ particles per second. The dust transport is then solved using a much larger time step, which is necessary because of the much larger dust mass. This transport creates space charge regions leading to instabilities. To adjust for this, the ion density profile is adapted to maintain quasi-neutrality. When too large a discrepancy between the new and the old solution occurs, the dust is frozen and the plasma equations are solved on the small sub-RF timescale to adapt to the new situation. This is repeated until final equilibrium is reached [34].

Magnetic field

In chapter 3, the above code is used to include the effect of a homogeneous axial magnetic field on the plasma transport, and investigate the effect of this on the formation of a void.

Charged particles gyrate around magnetic field lines, which reduces their mobility and diffusion coefficient perpendicular to the field. The degree to which the charged particles are prevented from crossing the magnetic field lines, is indicated by the Hall parameter; $H_j = \omega_j/\nu_{m,j} (= \mu_j B)$ [36], where $\omega_j = q_j B/m_j$ is the cyclotron frequency and $\nu_{m,j}$ is the momentum transfer frequency. The diffusion across magnetic field lines is strongly reduced (a particle species is magnetized) when $H_j > 1$.

For the ions we find in our argon discharge at 40 Pa background pressure $H_+ = \mu_+(40Pa)B = (133/40) \times 0.145 \times B = 0.48 B$. For the electrons, we find this way $H_e = \mu_e(40Pa)B \sim 100 B$ [32]. For the magnetic fields used in our simulations ($0.01 \leq B \leq 0.5 T$), we see that the ions are never magnetized, whereas the electrons always are. Therefore, we rewrite the mobility and diffusion coefficient for the electrons perpendicular to the magnetic field (thus in the radial direction) as:

$$\mu_{e,\perp} (D_{e,\perp}) \rightarrow \left[1 + \left(\frac{\omega_e}{\nu_{m,e}} \right)^2 \right]^{-1} \times \mu_{e,\perp} (D_{e,\perp}). \quad (2.68)$$

In the center of the discharge, quasi-neutrality and the particle balances result in *ambipolar* conditions that couple the ion flux to the electron flux via the average electric field that is generated. This means that the ion transport is also changed by a change in the electron transport.

2.4.2 Particle-in-Cell plus Monte Carlo

Using a fluid code as described above is useful for finding time and space averaged quantities. Such a code typically requires transport coefficients, while a certain energy distribution function for the electrons is assumed. If one wants to solve plasma at small length- or time-scales, or if one wants to find the energy distribution function (or does not want to assume one), a kinetic approach is necessary, such as the *Particle-In-Cell plus Monte Carlo* approach.

In this kind of modelling, one solves the motion of particles on a grid, solving their trajectories from the electrostatic force, which comes from the charge density the particles form on the grid. It is impossible to compute the motion of the huge amount of particles present in even the smallest plasmas. Therefore, *super-particles* are followed, which represent many real particles. The movement

of these particles is solved in the Particle-In-Cell module, whereas the collisions between charged plasma particles and the background gas, as well as the interaction between charged plasma particles and the dust, is solved in the Monte Carlo module.

In our model of a dusty RF discharge, we assume that the electrodes are parallel and infinite, which allows us to only consider the position of the particles on the central symmetry-axis, z , and the three velocity components v_x, v_y, v_z . Two dust clouds are fixed in position at two grid-point intervals within the discharge, but the dust charge density will vary, due to the collection of plasma by these dust clouds. The general approach is as follows [37]:

1. The charge q_j of every super-particle at position z_j is interpolated to the two nearest grid points.
2. The charge density on the grid ρ_k is calculated. The dust charge density on the grid $\rho_{k,D}$ is added, to find the total charge density on the grid $\rho_{k,tot} = \rho_k + \rho_{k,D}$.
3. The Poisson equation $\nabla_z^2 V_k = -\rho_{k,D}/\epsilon_0$ is solved to find the potential on the grid. The electric field in between the grid points is then found from $E_{k+\frac{1}{2}} = -\frac{V_{k+1}-V_k}{\Delta z}$.
4. The electric field found is then linearly interpolated to the nearest particles, to find the force acting on particle j ; F_j . Using a leapfrog scheme, the new velocity and position $v_{z,j}, z_j$ can then be found. Return to 1.

The above scheme enables us to follow the particles in space and time, but does not model a dusty plasma, since this requires collisions between plasma and neutrals, and between plasma and dust. To calculate this, we need the energy of the particles, which we get in step 4, from $E_j = mv_j^2/2$. From literature, we need the cross-sections for the i different collision processes $\sigma_i(E_j)$.

The average number of particles which experience a collision during a time-step Δt is calculated as follows. First, the total collision cross-section, which is the sum of all the collision cross-sections over the energy range considered in the code, is determined. The ion-neutral cross sections are taken from [38]. The electron collision cross-sections are taken from [39]. Then the corresponding total collision frequency is determined and the maximum is determined *once*,

$\frac{\nu_1(\epsilon_i)}{\nu_{max}}$	$<$	$U \leq \frac{\nu_1(\epsilon_i)}{\nu_{max}}$	Collision type 1
$\frac{\nu_1(\epsilon_i)}{\nu_{max}}$	$<$	$U \leq \frac{\nu_{max}(\nu_1(\epsilon_i) + \nu_2(\epsilon_i))}{\nu_{max}}$	Collision type 2
		\vdots	
$\sum_{j=1}^N \frac{\nu_j(\epsilon_i)}{\nu_{max}}$	$<$	U	Null collision

Table 2.1: The determination of the type of collision for every particle i from a total of N types of collisions.

$$\sigma_T(\epsilon) = \sigma_1(\epsilon) + \dots + \sigma_N(\epsilon) \quad (2.69)$$

$$\nu_T(\epsilon) = n_{gas} \sigma_T(\epsilon) \sqrt{\frac{2\epsilon}{m}} \quad (2.70)$$

$$\nu_{max} = n_{gas} max_{\epsilon} (\sigma_T(\epsilon) \sqrt{\frac{2\epsilon}{m}}) \quad (2.71)$$

The average fraction of particles experiencing a collision in the discharge within the time interval Δt is then given by,

$$P_{max} = 1 - \exp(-\nu_{max} \Delta t). \quad (2.72)$$

The colliding particles are randomly chosen from the total number of super-particles. For each particle is decided which kind of collision (assuming there are N different types of collisions) it will undergo, using a computer generated random number $U \in [0, 1)$, as shown in table 2.1. The "Null Collision" is an artificial collision, which changes nothing to the particle velocities. It only serves to keep ν_T constant over the whole energy range.

For the collisions with the dust particles a similar approach is followed, but now only between the boundaries of the dust clouds at z_1, z_2 , and z_3, z_4 . The cross-sections are given by [40],

$$\begin{aligned} \sigma_{capt} &= \min \left[\pi R^2 \left(1 \pm \frac{Q_d}{4\pi\epsilon_0 w_{+,e} R} \right), \pi L_{nn}^2 \right], \\ \sigma_{scat} &= \min(\pi \lambda_D^2, \pi L_{nn}^2) - \sigma_{capt}, \\ L_{nn} &= \left(\frac{3}{4\pi} \frac{1}{n_d} \right)^{1/3}, \\ \lambda_D^{-2} &= \lambda_e^{-2} + \lambda_+^{-2}, \end{aligned} \quad (2.73)$$

$$\lambda_{e,+}^2 = \frac{2\epsilon_0 \bar{w}_{e,+}}{3e^2 n_{e,+}}.$$

For collisions with the dust particles, the maximum collision frequency has to be calculated every time-step, since it depends on the dust charge, which changes every time-step. Once the type of collisions is chosen, the number of super-particles as well as the dust charge density within the clouds and the velocities of the colliding particles are updated.

When a collision occurs, the energy of the particles is changed (for instance in an ionization, the ionization potential is subtracted and the remaining energy divided over the two electrons), and the new velocity components are calculated, using computer generated random numbers for the angles. A complete description is given in [39, 41].

References

- [1] G. B. Rybicki, A. P. Lightman, *Radiative Processes in Astrophysics*, John Wiley & Sons, New York, 1979
- [2] F. F. Chen, *Introduction to plasma physics and controlled fusion*, Plenum Press, New York, 1984
- [3] A. Bogaerts, E. Neyts, R. Gijbels, and J. van der Mullen, *Spectrochim. Acta B* **57**, 609-658 (2002)
- [4] A. Bogaerts, and R. Gijbels, *J. Anal. At. Spectrom.* **15**, 1191-1201 (2000)
- [5] M. S. Barnes *et al.*, *Phys. Rev. Lett.* **68**, 313 (1992)
- [6] R. V. Kennedy, and J. E. Allen, *J. Plasma Physics* **69**, part. 6, 485-506 (2003)
- [7] R. V. Kennedy, and J. E. Allen, *J. Plasma Physics* **67**, part. 4, 243-250 (2002)
- [8] I. H. Hutchinson, *Principles of plasma diagnostics, first edition*, Cambridge University Press, Cambridge, 1987
- [9] M. Lampe, R. Goswami, Z. Sternovsky, S. Robertson, V. Gavriishchaka, G. Ganguli, and G. Joyce, *Phys. Plasmas* **10**, 1500 (2003)
- [10] S. A. Khrapak *et al.*, *Phys. Rev. E* **72**, 016406 (2005)
- [11] S. Ratynskaia *et al.*, *Phys. Rev. Lett.* **93**, 085001 (2004)
- [12] O. Havnes *et al.*, *J. Geophys. Res.* **92**, 2281 (1987)
- [13] M. Klindworth, *Fundamentals and Applications of Langmuir Probe Diagnostics in Complex Plasmas*, PhD. Thesis, Christian-Albrechts University, Kiel, 2004
- [14] D. A. Mendis, and M. Rosenberg, *Annu. Rev. Astron. Astrophys.* **32**, 419-463 (1994)

- [15] S. M. Lyth, F. Oyeleye, R. J. Curry, J. Davis, and S. R. P. Silva, *J. Vac. Sci. Technol. B* **24**, Issue 3, 1362 (2006)
- [16] W. I. Milne *et al.*, *J. Mater. Chem.* , 933-943 (2004)
- [17] R. C. Ister, R. W. Wood, C. C. Klepper, N. H. Brooks, M. E. Fenstermacher, and A. W. Leonard, *Phys. Plasmas* **4**, 355 (1996)
- [18] G. L. Delzanno, G. Lapenta, and M. Rosenberg, *Phys. Rev. Lett.* **92**, 035002 (2004)
- [19] H.-C. Wu, B.-S. Xie, *Phys. Plasmas* **12**, 064503 (2005)
- [20] M. R. Akdim, and W. J. Goedheer, *Phys. Rev. E* **67**, 066407 (2003)
- [21] J. E. Daugherty *et al.*, *J. Appl. Phys.* **73**, 1617 (1993)
- [22] S. A. Khrapak, A. V. Ivlev, G. E. Morfill, and H. M. Thomas, *Phys. Rev. E* **66**, 046414 (2002)
- [23] S. A. Khrapak, A. V. Ivlev, S. K. Zhdanov, and G. E. Morfill, *Phys. Plasmas* **12**, 042308 (2005)
- [24] A. V. Ivlev, S. K. Zhdanov, S. A. Khrapak, and G. E. Morfill, *Plasma Phys. Control. Fusion* **46**, B267-B279 (2004)
- [25] A. V. Ivlev, S. K. Zhdanov, S. A. Khrapak, and G. E. Morfill, *Phys. Rev. E* **71**, 016405 (2005)
- [26] I. H. Hutchinson, *Plasma Phys. Control. Fusion* **48**, 185-202 (2006)
- [27] P. S. Epstein, *Phys. Rev.* **23**, 710 (1923)
- [28] S. A. Khrapak, and G. E. Morfill, *Phys. Plasmas* **13**, 104506 (2006)
- [29] O. Arp, D. Block, M. Klindworth, and A. Piel, *Phys. Plasmas* **12**, 0122102 (2005)
- [30] G. Gozadinos, A. V. Ivlev, and J. P. Boeuf, *New J. Phys.* **5**, 32 (2003)
- [31] G. E. Morfill, H. M. Thomas, U. Konopka, H. Rothermel, M. Zuzic, A. Ivlev, and J. Goree, *Phys. Rev. Lett.* **83**, 1598-1601 (1999)
- [32] J. D. P. Passchier, *Numerical Fluid models for RF discharges*, PhD. Thesis, University Utrecht, 1994
- [33] G. J. Nienhuis, *Plasma models for silicon deposition*, PhD. Thesis, University Utrecht, 1998
- [34] M. R. Akdim, *Modelling of Complex Plasmas*, PhD. Thesis, University Utrecht, 2003

- [35] I. Revel *et al.*, J. Appl. Phys. **88**, 2234 (2000)
- [36] E. W. McDaniel, *Collision phenomena in ionized gases*, John Wiley & Sons, New York, 1964
- [37] C. K. Birdsall, and A. B. Langdon, *Plasma Physics via Computer Simulation*, Adam Hilger, New York, 1991
- [38] W. H. Cramer. J. Chem. Phys. **30**, 641 (1959)
- [39] V. Vahedi, M. Surendra, Comp. Phys. Com. **87**, 179-198 (1995)
- [40] W. J. Goedheer, Y. I. Chutov, IEEE Trans. Plasma Sci. **32**, 606-613 (2003)
- [41] M. H. L. van der Velden, W. J. M. Brok, J. J. A. M. van der Mullen, W. J. Goedheer, and V. Banine, Phys. Rev. E **73**, 036406 (2006)